BỘ GIÁO DỤC VÀ ĐÀO TẠO

**TRƯỜNG ĐẠI HỌC MỎ - ĐỊA CHẤT**

---

# BÁO CÁO SINH HOẠT HỌC THUẬT

Tên báo cáo:

# Geological setting and mineralization characteristics of the Tick Hill Gold Deposit, Mt Isa, Queensland, Australia

Cơ quan chủ trì: Trường Đại học Mỏ - Địa chất

Chủ nhiệm báo cáo: TS. Lê Xuân Trường

**Hà Nội, 12/2022**

## Acknowledgements

I would like to thank all the people involved in thí Tick Hill Project. First and foremost, I would like to express special thanks to Professor Paul Dirks, Dr. Ioan Sanislav and Dr. Jan Huizenga who has given me great support throughout the project.

My thanks also extend to personnel of the Geological Survey of Queensland (GSQ), the Economic Geology Research Centre (EGRU) - James Cook University, Rick Valenta and the Hanoi University of Mining and Geology (HUMG) who provided much appreciated support in helping me conduct this study. I would like to thank Mr. Peter Rea and Alex Brown from Glencore, Mount Isa Mines, and Mr. Paul Tan, Brett Davis and Rob Watkins from Carnaby Resources for providing logistical support for fieldwork, access to drill core and data sets. My thanks to Nick Oliver for donating Tick Hill samples for this study. My thanks to Dr. Kaylene Camuti for help with editing early versions of the manuscripts. Funding for this study was provided by the Department of Natural Resources, Mines and Energy, as part of the northwest minerals province program. I would like to thank Ms. Judith Botting (EGRU) and Ms. Rebecca Steel, Ms. Debbie Berry, Mr. Alex Salvador and Ms. Katherine Elliott (JCU) for their help in administrative work. I would like to acknowledge Dr. Yi Hu and Dr. Huang Huiqing from JCU for their help with LA-ICP-MS zircon dating. I would further like to extend my thanks to the SEM-EPMA-Geochemistry experts, Dr Kevin Blake and Dr. Shane Ankew, in the Advanced Analytical Centre - JCU for their assistance in helping me with geochemical analyses. My thanks to Pof. Chris Harris, University of Cape Town (UCT), South Africa for his contribution in oxygen isotope analysis.

# Table of Contents

# Geological setting and mineralization characteristics of the Tick Hill Gold Deposit, Mount Isa Inlier, Queensland, Australia


## Abstract

The high grade (~22.5 g/t), gold-only Tick Hill deposit presents a unique mineralization style in the Mt Isa Inlier. The deposit was mined in the early 1990s, and is hosted in biotite schist, calc-silicate gneiss, quartzite and quartzo-feldspar mylonite. These rocks were affected by $D_1$ shearing and $D_2$ upright folding at high-grade metamorphic conditions, followed by $D_3$ normal faulting with widespread quartz-feldspar alteration and $D_4$ strike-slip faulting. The Tick Hill ore body is linear in shape and paralleled the $D_1$ mineral elongation lineation, and the intersection lineation between sets of $D_3$ faults. Gold is dominantly hosted within intensely silicified units affected by $D_3$ fracturing and associated alteration. Some gold grains are contained within syn-$D_1$, peak-metamorphic minerals indicating that mineralization involved two separate events; an early event predating or concomitant with $D_1$ when gold was first introduced and concentrated, and a second event during $D_3$ when gold was remobilized and/or further enriched to be deposited in its final configuration. Mineralization at Tick Hill is characterized by coarse grained gold associated with Bi-selenides, minor sulfides, and a general paucity of other metals except for a slight enrichment of Cu in the footwall to the ore zone. Alteration is characterized by early silicification and magnetite alteration that formed during the initial $D_{1-2}$ events and may have coincided with the first stage of gold enrichment. During syn-$D_3$ mobilization of gold, alteration involved the destruction of magnetite, the emplacement of abundant laminar quartz veins, and the deposition of proximal albite, hematite, chlorite, amphibole, epidote overprinted by later K-feldspar, sericite, clay minerals and minor calcite. The ore zone is bounded by a strongly silicified zone and surrounded by a chlorite-epidote shell. The low pressure (< 1 kbar) $D_3$ gold mobilization event involved an oxidized, S-under-saturated, acidic, saline aqueous fluid. In terms of alteration characteristics, the Tick Hill deposit shares similarities with IOCG deposits in the area. However, its high-grade gold-only nature, lack of Cu, and the presence of Bi-selenides makes it a unique deposit in the Mt Isa Block. Textural evidence suggests that early gold enrichment existed in the area, and that later metasomatic fluids may have mobilized this gold into suitable structural traps during $D_3$.


## 1. Introduction

The Mesoproterozoic (1900-1500 Ma) Mt Isa block is one of Australia's foremost mineral provinces and is famous for its world-class SEDEX-type, Cu-Pb-Zn-Ag (e.g. Mt Isa mine; Huston et al., 2006), structurally modified and metamorphosed SEDEX (e.g. Dugald River, Cannington; Xu, 1996; Walters and Bailey, 1998) and Cu-Au IOCG deposits (e.g. Ernest Henry; Mark et al., 2006). In addition to these, there are many other large deposit including Mo (e.g. Merlin; Babo et al., 2017), Co (Walford Creek; Aeon Metal Limited, 2017), REE/U (Mary Kathleen; Oliver et al., 1999) and gold-rich IOCG's deposits (e.g. Starra; Duncan et al., 2014).

The Mt Isa block also represents one of the most extensively altered terrains on Earth exemplified by widespread albite-hematite-scapolite-epidote alteration, which is linked to the remobilization of evaporite deposits during various deformational and intrusive events (e.g. Oliver et al., 1994; Oliver, 1995; De Jong and Williams, 1995; Withnall and Hutton, 2013). This alteration is accompanied by widespread brecciation, and the syn- to post-tectonic emplacement of both felsic and mafic intrusions (e.g. Oliver, 1995; Oliver et al., 2008). The alteration and brecciation are characteristic features of the IOCG deposits in the Mt Isa Block (Williams et al., 2005) and are hallmarks for many of the other deposit types as well.

Whilst Cu-Au deposits are common in the Mt Isa block, especially in the higher grade and more strongly deformed Eastern Fold Belt (Fig. 1.1, Chapter 1), gold grades in such deposits rarely exceed 1-2 g/t, and gold-rich deposits are rare (e.g. Duncan et al., 2011; Denaro et al., 2013). One notable exception to this is the Tick Hill gold deposit in the southern part of the Mary Kathleen Domain (MKD; Fig. 1.1, Chapter 1). Although the Tick Hill deposit presents a mineralization style of great interest to exploration companies, little is known about the deposit other than that it is a gold-rich, shear-hosted hydrothermal deposit (Denaro et al., 2013) that has been interpreted as a possible end-member IOCG deposit (e.g. Groves et al., 2010). Tick Hill was discovered in 1989, and was mined over a short period of time (1991-1994). Apart from several student theses (Tedman-Jones, 1993; Watkins 1993; Choy, 1994) no detailed studies have been published on the deposit or its style of mineralization.

The high-grade Tick Hill deposit is situated in high-grade metamorphic rocks and characterized by the occurrence of free gold with little to no silver and a paucity of sulphides and associated metals (e.g. Cu, Co). As such, Tick Hill is a unique gold-rich deposit in the Mount Isa Inlier, which was highly profitable when mined. This study provides an overview of the geological setting and mineralization style of the Tick Hill deposit based on mapping, core logging and petrography. It aims to present details on the orebody geometry in relation to lithological and structural-metamorphic controls, together with a characterization of the gold mineralization and associated alteration.

## 2. Geological setting

### *2.1. Regional geological setting*

The Mount Isa Inlier in northwest Queensland exposes complexly deformed, strongly altered and extensively mineralized, mid-Proterozoic rocks that comprise at least three separate basinal sequences (originally referred to as Cover Sequences 1 to 3; Blake, 1987) deformed by two orogenic cycles (Etheridge et al., 1987; Foster and Austin, 2008). The inlier was originally sub-divided into three, north-trending tectonic units including the Western Fold Belt, the central Kalkadoon-Leichhardt Belt and the Eastern Fold Belt (Day et al., 1983), to delineate large-scale subdivisions with broadly similar tectono-stratigraphic histories. These subdivisions were further split into a series of geological domains based on stratigraphic, structural and

geochronological similarities (Fig. 1.1, Chapter 1; Withnall and Hutton, 2013). Thus, the Eastern Fold Belt, which occurs east of the Kalkadoon-Leichardt Domain, comprises eight domains including the MKD that hosts the Tick Hill deposit (Fig. 1.1, Chapter 1). To the west, the metasedimentary rocks of the MKD uncomfortably overlie rocks of the Kalkadoon-Leichhardt Domain (Withnall and Hutton, 2013). To the east, the MKD is separated from the rest of the Eastern Fold Belt by the Pilgrim fault in the south and the Rose Bee fault in the north (Withnall and Hutton, 2013).

The Tick Hill deposit is situated in the southern part of the MKD. This part of the MKD is relatively poorly studied and stratigraphic and tectonic interpretations for rocks around Tick Hill largely rely on lateral correlations with better studied rocks further north (e.g. Passchier, 1986, 1992; Passchier and Williams, 1989; Holcombe et al., 1991; Neumann et al., 2009; Carson et al., 2011; Withnall and Hutton, 2013; Kositcin et. al., 2019). In the central part of the MKD, gneiss of the Kalkadoon-Leichhardt complex, and overlying mafic and felsic volcanics of the Magna Lynn metabasalt unit, and the 1770-1780 Ma Argylla Formation (e.g. Page, 1978; Foster and Austine, 2008, Neumann et al., 2009; Fig. 2.1), form basement to unconformably overlying shallow water sediments (e.g. Witnall and Hutton, 2013). These consist of the ca. 1755 Ma Ballara Quartzite and extensive deposits of the 1738-1750 Ma Corella Formation (Blake et al., 1982; Foster and Austin, 2008; Neumann et al., 2009; Withnall and Hutton, 2013; Kositcin et. al., 2019; Fig. 2.1). In the central MKD, the Corella Formation is composed of shallow marine sediments, including scapolitic-bearing calc-silicate, para-amphibolite, calcite marble, metapelite, quartzite and other metasedimentary units with minor felsic and mafic metavolcanics (Blake, 1987; Foster and Austin, 2008). The correlative stratigraphic unit of the Corella Formation in the area around Tick Hill has not been dated directly and its age has been interpreted (e.g. Wyborn 1997; Foster and Austin, 2008). Intrusions in the southern MKD have been grouped into granites assigned to the ca. 1740 Ma Burstall-Wonga suite (e.g. Monument syenite, Saint Mungo granite, Birds Well granite and Tick Hill granite; Fig. 2.2) and Kalkadoon batholith, which mostly occurs to the W of Tick Hill (e.g. Blake et al., 1982; Wyborn, 1997; Withnall and Hutton 2013).

The metamorphic and deformational history of the MKD involved four major deformational events ($D_1$ to $D_4$; e.g. Passchier and Williams, 1989; Holcombe et al., 1991; Oliver, 1995). The early $D_1$ event (1750-1730 Ma) is thought to be extensional in nature and has been linked to an early gneissic fabric exposed in high strain zones along the central part of the MKD termed the Wonga-Shinfield zone (Passchier and Williams, 1989; Holcombe et al., 1991). Upright folding occurred during $D_2$ and was originally interpreted to relate to the main stage of the Isan Orogeny around 1590-1550 Ma, when peak metamorphic conditions were attained (e.g. Page, 1983; Passchier and Williams, 1989; Holcombe et al., 1991; Oliver, 1995). More recently, however, Spence et al. (2020) have shown that $D_2$ upright folding in the central MKD took place before 1710 Ma. The $D_2$ deformation resulted in the development of upright, tight, north-trending folds with an axial planar cleavage, a penetrative $S_2$ fabric, and steep east-dipping reverse faults parallel to $F_2$ fold axial planes (e.g. Holcombe et al., 1991; MacCready et al., 1998). $D_3$ events marked a change from ductile to brittle deformation and led to

the formation of a fault network (O'Dea et al., 1997; Betts et al., 2006). In the southern MKD, the Wonga-Shinfield zone was offset by a series of northeast and northwest striking $D_3$ faults in response to east-west compression (Forrestal et al., 1998). $D_3$ events were coeval with the regional emplacement of the Wimberu/Williams granite plutons (1530-1500 Ma; Foster and Austin, 2008) to the east and related regional albite-hematite- alteration (Wyborn et al., 1988). $D_4$ events involved brittle reactivation of older fault zones at shallow crustal levels, at temperatures less than 350-400$^{o}$C, with the age of deformation ranging from 1500 Ma to 1100 Ma (e.g. Oliver, 1995).

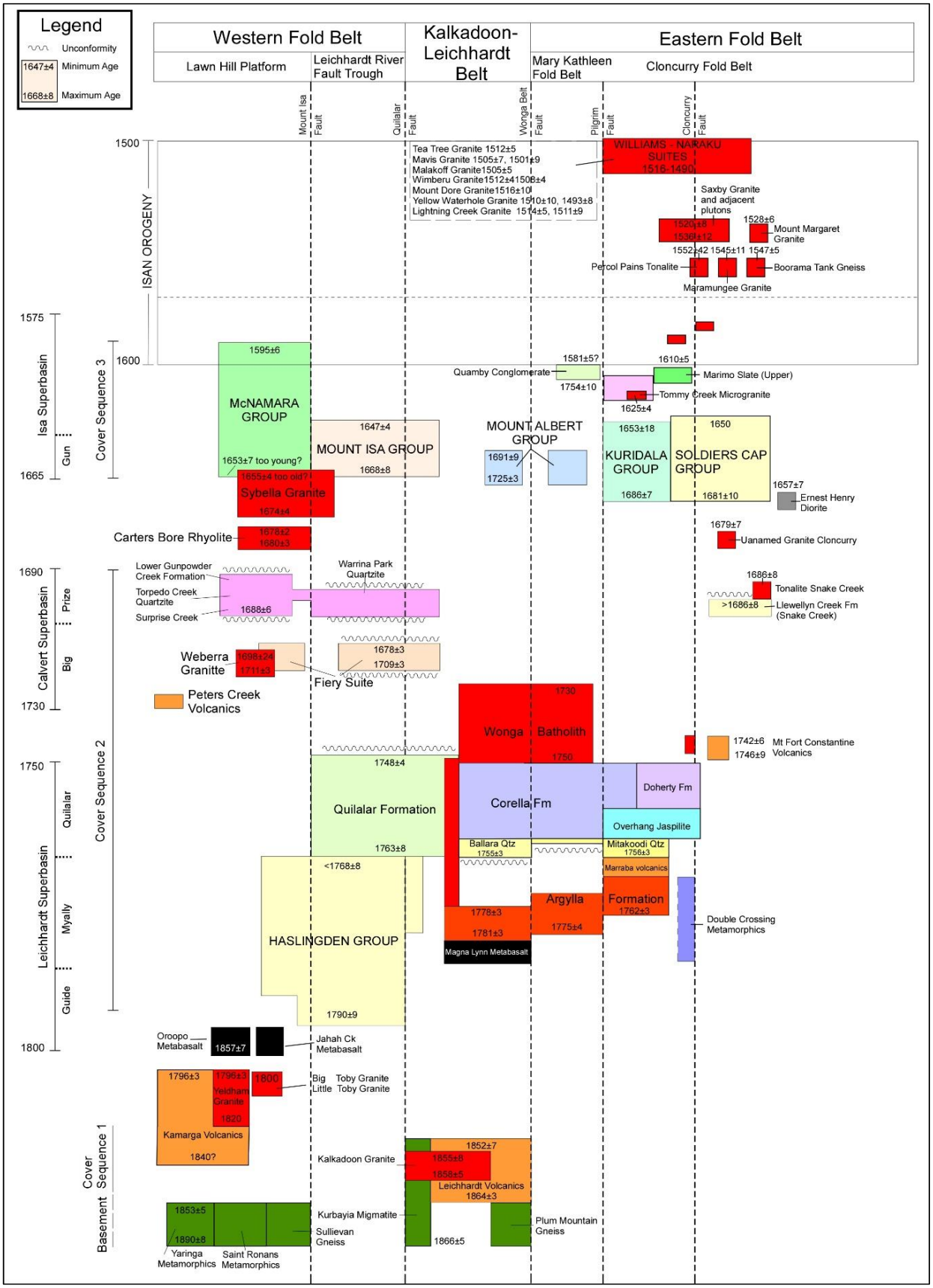


Figure 2.1. Chronostratigraphic time-space plot for the Mt Isa Inlier (after Foster and Austin, 2008; Withall and Hutton, 2013).

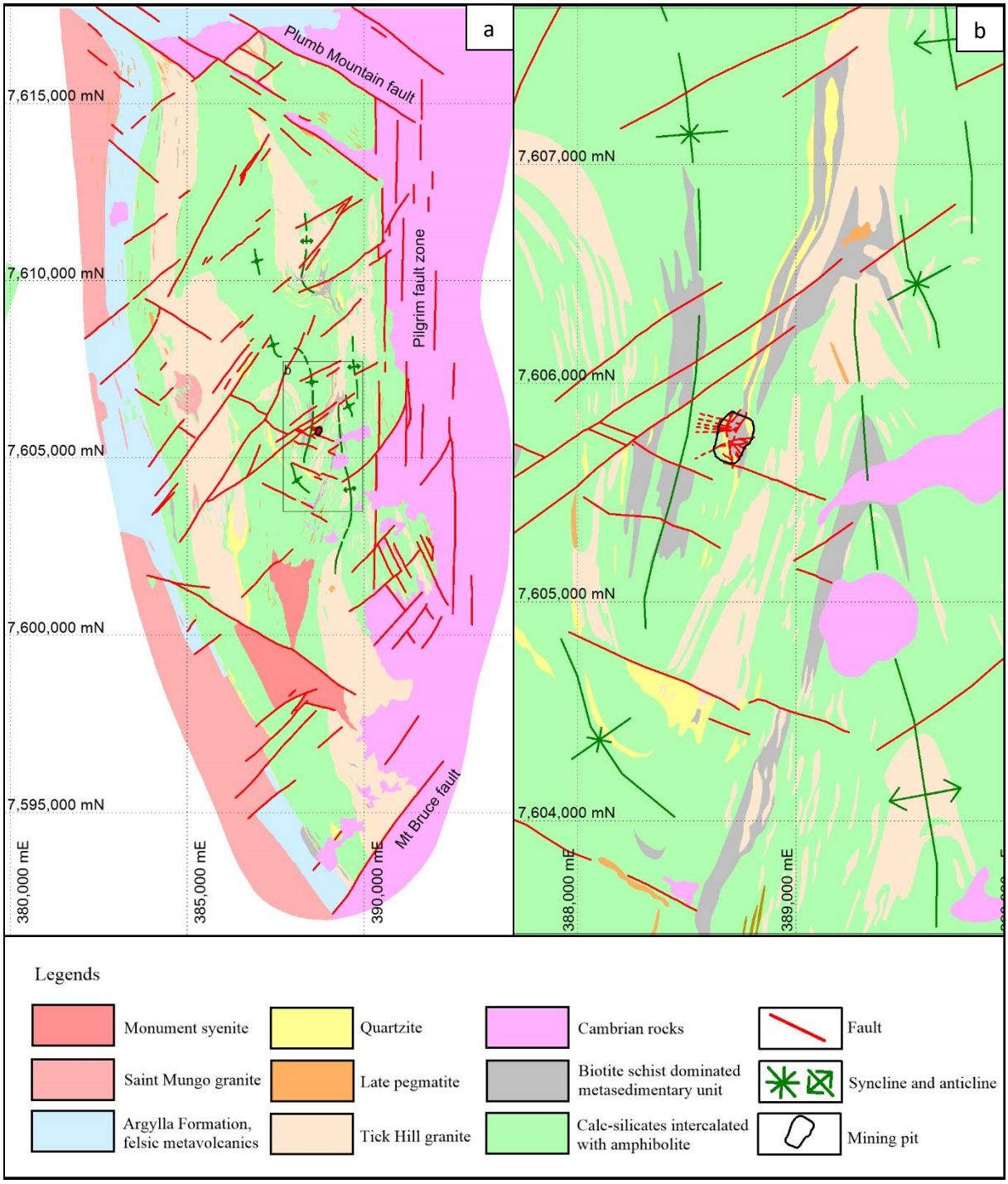


*Figure 2.2. (a) Geological map of Tick Hill Area with (b) a close-up of the Tick Hill Syncline. Note that the calcsilicate, amphibolite, biotite schist and quartzite units were interpreted as the Corella Formation while the felsic metavolcanics were assigned to the Argylla Formation (adapted from Wyborn, 1997; Rutherford, 2000).*

### *2.2. Geological setting of the Tick Hill Area*

The Tick Hill area is underlain by rocks mapped as Corella Formation bounded in the east by the Pilgrim fault and in the west by granitic gneiss of the Saint Mungo granite overlain by Argylla Formation (Coughlin, 1993; Wyborn, 1997). To the north, the area is bounded by the northwest-trending Plumb Mountain fault and

to the south by the northeast-trending Mt Bruce fault (Forrestal et al., 1998; Fig. 2.2a). The rocks of the Corella Formation were intruded by syn- to post-tectonic granite plutons and pegmatites of the Tick Hill Complex (Wyborn, 1997) and Monument Syenite (Fig. 2.2a, Rutherford, 2000). Cambrian rocks outcrop to the east of the Pilgrim fault and are locally preserved as erosion remnants overlying the Corella Formation to the east of the Tick Hill pit (Fig. 2.2a).

Detailed mapping of the Tick Hill Area and the surrounding geology during exploration by MIM (Fig. 2.2; Coughlin, 1993; Rutherford, 2000) led to the development of a $D_1$ to $D_4$ deformation sequence that was linked to the regional tectonic framework further north. Around Tick Hill, $D_1$ refers to the development of the mylonitic gneissic fabric that hosts the Tick Hill deposit. The mylonite formed along a north-trending belt, west of the Pilgrim fault, and is characterized by a prominent $S_1$ foliation with a westerly dip (around 280/60; all orientation measurements for planes are presented as dip direction/dip) and a well-developed steeply southwest pitching mineral lineation and/or rodding lineation ($L_{1x}$). The fabric is defined by oriented hornblende-plagioclase-clinopyroxene assemblages in metabasalt and silimanite-biotite-scapolite in meta-sediments. Numerous quartzo-feldspathic horizons and sheared leucogranite layers suggest the presence of abundant granite melt pockets, either formed as the result of local migmatisation, granite intrusions or both (Fig. 2.2). Intrafolial folds and sheath folds in the mylonitic fabric can be observed on centimeter to meter scale, and in places several overprinting generations of intrafolial folds have been described (e.g. Choy, 1994; Oliver, 1998). $F_1$ fold axes associated with the intrafolial folds are commonly parallel to the mineral lineation. The $D_1$ high strain fabric has been linked to the Shinfield-Wonga belt north of Tick Hill (Oliver, 1998). By inference, this fabric was interpreted as an expression of the ca. 1740 Ma, mid-crustal extensional shear zone (e.g. Oliver, 1998). The $D_1$ mylonites were folded during $D_2$ in a series of km-scale, tight, asymmetric upright folds. The Tick Hill deposit is situated in the eastern limb of one such large $D_2$ syncline (the Tick Hill syncline; Fig. 2.2b), which has an axial planar trace that largely parallels the $D_1$ gneissic fabric (Choy, 1994). The $D_2$ folds tighten and intensify west of the Tick Hill pit, where they become transposed in a north-trending high strain zone that parallels the $S_1$ fabric, suggesting that $D_1$ and $D_2$ events may be expressions of a single, progressive shearing event (Laing, 1993). $D_2$ folds open up towards the Pilgrim fault to the east. Later deformation events ($D_3$ and $D_4$) were described as northwest- and northeast-trending normal fault sets with associated red rock alteration (Tedman-Jones, 2001). The main $D_3$ structures bound the Tick Hill Area to the north and south (Fig. 2.2). Within the deposit, $D_3$ is manifested as an interconnected network of fractures and veins with associated quartz-feldspar alteration and gold mineralization (Tedman-Jones, 2001). $D_4$ deformation includes a series of strike-slip faults that trend northeast, and offset the $D_1$ Tick Hill gneiss fabric and $D_2$ fold axes (Coughlin, 1993), and overprinted the $D_3$ red rock alteration (Tedman-Jones, 2001).

## 3. Geological framework for the Tick Hill Deposit

The deformation scheme and lithological descriptions presented here are based on mapping of the Tick

Hill pit in November 2017, together with drill core logging of a limited number of available cores, and petrological studies. This is augmented with regional maps compiled by MIM in the 1990's (Fig. 2.2; Coughlin, 1993; Rutherford, 2000).

### *3.1. Lithological units in Tick Hill Pit*

The host rocks to the Tick Hill deposit as exposed in the pit and its immediate surroundings, consist of gneissic and schistose units that have been interpreted as part of the Corella Formation (e.g. Coughlin, 1993; Choy, 1994; Wyborn 1997, Figs. 2.2, 2.3). They include from west to east (i.e. from hanging wall to footwall): (1) a hanging wall calc-silicate unit interlayered with amphibolite gneiss, (2) hanging wall quartzite, (3) a central metasedimentary unit dominated by biotite schist, (4) footwall quartzite, and (5) footwall calc-silicate interlayered with amphibolite gneiss. The ore zone is largely contained within the central biotite schist unit, where it is interlayered with quartzo-feldspathic gneiss that is similar in composition as the nearby Tick Hill Granite Complex (Chapter 3) and probably of intrusive origin. The origin of the quartzite ridges is uncertain, and most exploration reports refer to them as metasomatic alteration zones, rather than sedimentary units, citing their cross-cutting, discontinuous nature (e.g. Laing, 1993; Coughlin, 1993; Oliver, 1998). All units are truncated by weakly deformed quartz and pegmatite veins. The distribution of the various lithologies in the pit is presented in Fig. 2.3 and the peak-metamorphic mineral assemblages in each rock unit are listed in Table 2.1.

*Hanging wall calc-silicate interlayered with amphibolite gneiss*

This unit is well-exposed in the west wall of the pit, and in many drill cores. The unit comprises banded or laminated gneissic calc-silicate and amphibolite, interbedded with lesser biotite schist, and can be sub-divided into amphibolite, amphibole-rich calc-silicate, calc-silicate, and magnetite-rich calc-silicate sub-units (Fig. 2.4).

The gneissic amphibolite sub-unit is best exposed along the top benches of the open pit where it overlies calc-silicate (Fig. 2.3a). The amphibolite is strongly foliated, with the foliation defined by oriented hornblende, which comprises ~50-80% of the rock (Figs. 2.4a, 2.5a). Other minerals include plagioclase, scapolite, quartz, magnetite, actinolite, garnet and accessory minerals including zircon and apatite (enclosed in quartz). Locally, the amphibolite sub-unit displays variations in composition on m-scales, with quartz-rich (>10% quartz) amphibolite horizons alternating with plagioclase-rich or calc-silicate-rich horizons.

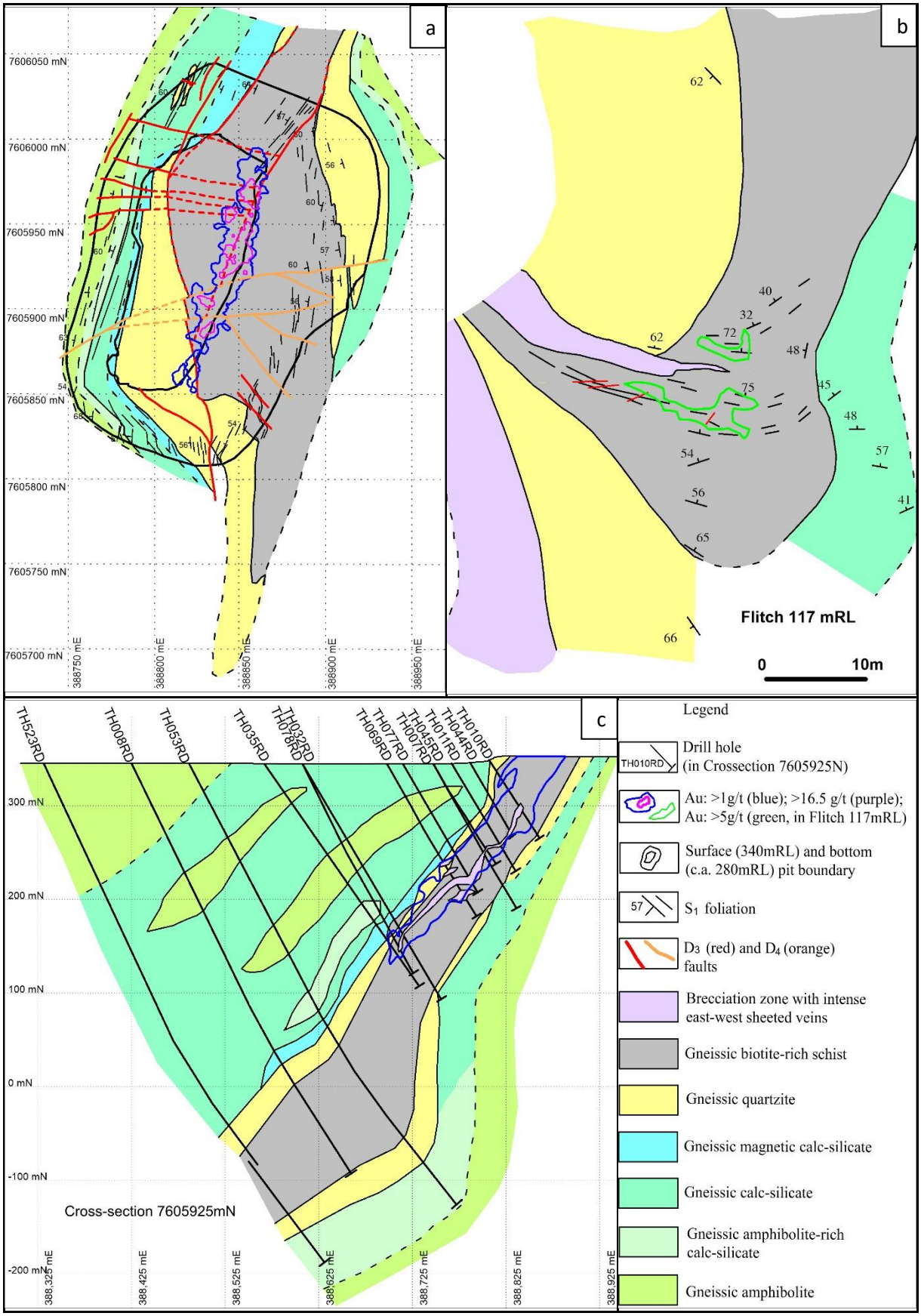


*Figure 2.3. Geology of the Tick Hill deposit. (a) Geological map of Tick Hill Pit as exposed in November 2017. The surface elevation responds to mine level 340 mRL; (b) Underground geological map of level 117 mRL towards the base of the mine, showing folded layering and a shift of the ore zone from a north-northeast trend*

*at surface to an east-trend (adapted from MIM, 1993); (c) Cross-section 7605925 mN showing the lithological host rocks in spatial relationship with the 1g/t ore envelope and brecciation zones. Drill holes are projected onto the section from 20m north and south (adapted from Downs, 2000). The 1g/t ore envelope is hosted in biotite schist and hanging wall quartzite. Brecciation with emplacement of east-west sheeted veins coincided with the ore envelope.*

The gneissic calc-silicate sub-unit (Fig. 2.4b) constitutes the bulk of the rock in the sequence above the hanging wall quartzite, and is well-exposed in the west wall of the pit (Fig. 2.3a). The general composition of the calc-silicate is feldspar (40-60%), scapolite (20-35%), quartz (10-15%), magnetite (<3-4%) and variable amounts of hornblende, actinolite and chlorite (e.g. Fig. 2.5b). The scapolite content is highly variable from one layer to the next. Where scapolite is most abundant it preserves a spotty texture, with individual grains aligned within the foliation. Hornblende occurs in discontinuous patches along the mylonitic foliation and locally defines the mineral lineation (Fig. 2.4b). Amphibole-rich layers consisting of quartz-feldspar-amphibole (± scapolite, biotite, and magnetite) occur as intervals in the more massive calc-silicate sequence. The calc-silicate sub-unit is generally altered and overprinted by sericite and clay after feldspar, and chlorite-hematite-goethite after amphibole-biotite-magnetite. Layers of biotite-schist are locally intercalated with the calc-silicate, but they are too thin and laterally too discontinuous to be mapped as separate units.

The magnetite-rich calc-silicate sub-unit occurs directly above the hanging wall quartzite unit and locally reaches a thickness of 30m. This sub-unit is similar in composition to calc-silicate except that the magnetite content is much higher. In drill core (e.g. Geological Survey of Queensland, 2015), the magnetite concentration increases toward the contact with the hangingwall quartzite, to form a 4-6 m wide contact zone consisting of discontinuous, semi-massive to massive granular magnetite lenses (Fig. 2.4c). The magnetite-rich calc-silicate is locally intercalated with thin bands of magnetite-bearing amphibolite. Magnetite is aligned in the gneissic fabric and appears to have formed as an early alteration product overprinting and replacing the dominant rock forming minerals, as shown by the presence of abundant aligned magnetite replacing biotite along the $S_1$ fabric.

*Hanging wall quartzite*

The hanging wall quartzite unit is best exposed in the southern wall of the pit, and in drill cores. The hanging wall quartzite has been intensely deformed and in the immediate hanging wall to mineralization it has been affected by quartz-feldspar alteration. The unit is gray-white in colour and dominated by quartz, but it varies in the composition of secondary minerals that occur as inclusions in quartz. As a result, the quartzite can be locally enriched in biotite, or hornblende-chlorite-epidote or feldspar, with inclusion phases aligned in the gneissic layering and partly overgrown by quartz (Fig. 2.4d). The quartzite is magnetite-bearing along the contact with the overlying calc-silicate unit, but the magnetite content of the rock decreases away from the contact, to form a weakly magnetic middle interval of glassy quartzite. This middle interval is

discontinuous along strike, and the magnetite-rich quartzite locally occurs directly above the mineralized zone, especially in amphibolite-rich areas. Intercalations of silicified biotite schist are locally common. The hanging wall quartzite displays an annealed granoblastic texture, in which the dominant foliation is only weakly preserved. It can be intensely brecciated and pervasively altered resulting in a spotty texture. The effects of this alteration are well exposed in the upper benches in the southeast corner of the pit (Fig. 2.3a). Where alteration is prevalent, chlorite and hematite appears, and feldspar has been altered to sericite and clay minerals.

*Biotite schist*

The biotite schist unit is well exposed in the north wall of the pit, and is a major host rock to mineralization. However, the strongly altered and mineralized varieties of this unit (including the high-grade ore zones or "galahstone") can only be seen in drill cores. The biotite schist unit is located between the hanging wall and footwall quartzite units (Fig. 2.3a), and comprises three sub-units: (1) quartz-feldspar-biotite-amphibole schist (i.e. meta-psammite); (2) biotite-schist that locally contains sillimanite (i.e. meta-pelite), and (3) quartz-feldspar mylonite, which is probably of intrusive origin and commonly gold-rich (see Chapter 3). Other minor intercalations include amphibolite gneiss and quartzite.

The quartz-feldspar-biotite-amphibole schist sub-unit occurs along the base of the hanging wall quartzite, between the quartzite and the ore zone. The transition from the hanging wall quartzite to biotite schist is gradational and the exact contact is masked by silicification. The least altered parts of this sub-unit contain a fine-grained, light-tan, massive to weakly foliated arkose siltstone or arenite (Fig. 2.4e). The composition varies laterally and includes quartz (35-60%, including secondary quartz due to silicification), feldspar (15-20%), biotite (5-20%), amphibole (10-20%) and magnetite (± ilmenite, 2-3%). Oriented biotite, amphibole and quartz define a strong schistose fabric.

Biotite schist commonly occurs below the quartz-feldspar-biotite-amphibole schist, close to or coinciding with the high-grade ore zone, and it extends into the footwall of the ore zone. Biotite-rich varieties occur along layers, and sillimanite is locally abundant, especially in footwall zones to the ore body (Fig. 2.4f), although much of the sillimanite has been replaced by muscovite. Within the ore zone, the biotite schist has been intensely silicified, and chlorite-hematite altered (TH76) and the older mylonitic texture was strongly recrystallized into an interlocking texture of granoblastic quartz grains. The biotite sub-unit generally consists of fine- to coarse-grained biotite and/or biotite-amphibole (30-80%), with quartz (<30%) and feldspar (K-feldspar and plagioclase, <50%) that was partially altered to sericite and clay minerals; Fig. 2.5d).

The quartz-feldspar mylonite sub-unit is the principle host to gold mineralization in the sequence and occurs as layers within biotite schist. It consists of equal amounts of quartz and feldspar (albite and oligoclase) that occur as discontinuous ribbon grains interlaminated with thin quartz bands (Figs. 2.4i, 2.5e). Individual

quartz and feldspar lamellae generally do not exceed 3 mm in width, and they are mostly thinner than that, but in places quartz-rich or feldspar-rich bands (or veins) can be up to 10 cm thick. Feldspar consists of albite with minor K-feldspar and Na-rich oligoclase. The quartz-feldspar mylonite is characterized by a sugary, granoblastic texture reflecting post-deformational annealing and recovery (Fig. 2.5f). In places, the recrystallized fine-grained quartz-feldspar mylonite is truncated by, or overprinted by laminated thin (< 2 mm) partings of grey quartz, which formed parallel or at low angles to the original mylonitic foliation (i.e. the "laminate" of Laing, 1992). The composition of the quartz-feldspar mylonite suggests that it originated as intrusive granite sheets or granitic migmatite (Chapter 3).

*Footwall quartzite*

This unit is best exposed in the northeast corner of the pit. Most drill cores do not penetrate this unit, limiting descriptions to field observations. The thickness of the footwall quartzite varies along strike and with depth and it pinches out towards the south end of the pit (Fig. 2.3a). The unit is thickly bedded (>30cm), and consists of grey-white translucent orthoquartzite (Fig. 2.4k) with traces of biotite, magnetite and heavy minerals including zircon and apatite. The unit has a granoblastic texture with a common grain size of 150-350 μm, and has been strongly deformed, but it lacks the spotty texture resulting from abundant inclusions of feldspar, magnetite, hornblende or biotite, and alteration, which characterizes the hanging wall quartzite.

*Footwall calc-silicate interlayered with amphibolite gneiss*

This unit is not exposed in the pit, and few drill cores penetrate it. The unit is similar in appearance to the various calc-silicate and amphibolite lithologies described above. In the immediate footwall to the footwall quartzite unit, calc-silicate lithologies dominate, whilst away from the quartzite the unit is transitional into amphibolite (Fig. 2.3a).

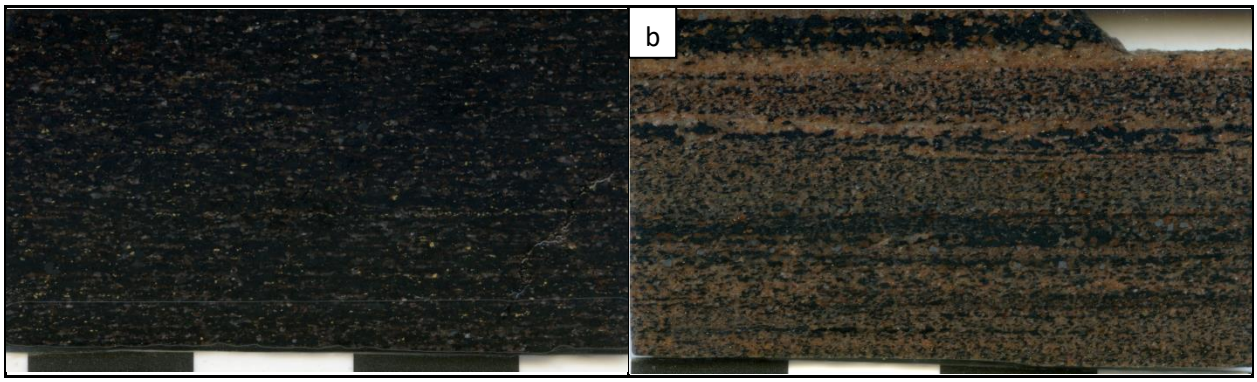

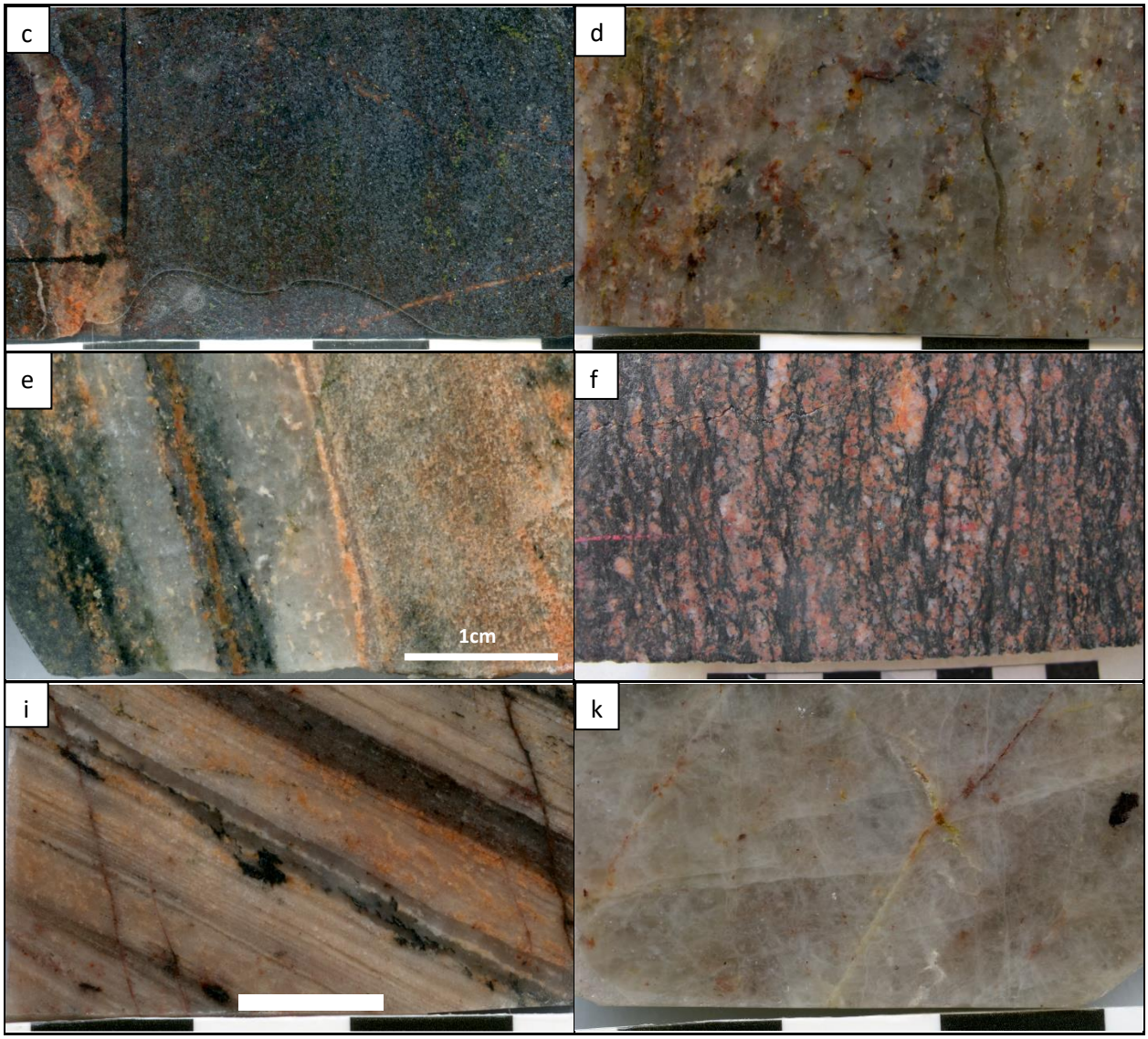


*Figure 2.4. Rock units from Tick Hill. (a) Gneissic amphibolite composed of amphibole and plagioclase defining $S_1$; (b) Gneissic calc-silicate composed of amphibole, scapolite, plagioclase defining $S_1$; (c) Amphibole-rich calc-silicate consisting of amphibole-rich bands interlayered with calc-silicate bands that consist of amphibole-quartz-plagioclase-scapolite-magnetite; (d) Hanging wall quartzite showing distributed feldspar grains affected by quartz alteration; (e) Quartz-feldspar-biotite-amphibole schist sub-unit within the biotite schist; (f) Biotite schist in the pit wall composed by biotite, feldspar, sillimanite and amphibole, overprinted by red-rock alteration; (i) Typical quartz-feldspar mylonite, with feldspar-quartz laminae intercalated with thin quartz vein that have the appearance of ribbon grains. (k) Foot wall quartzite composed of strongly recrystallized granoblastic quartz.*

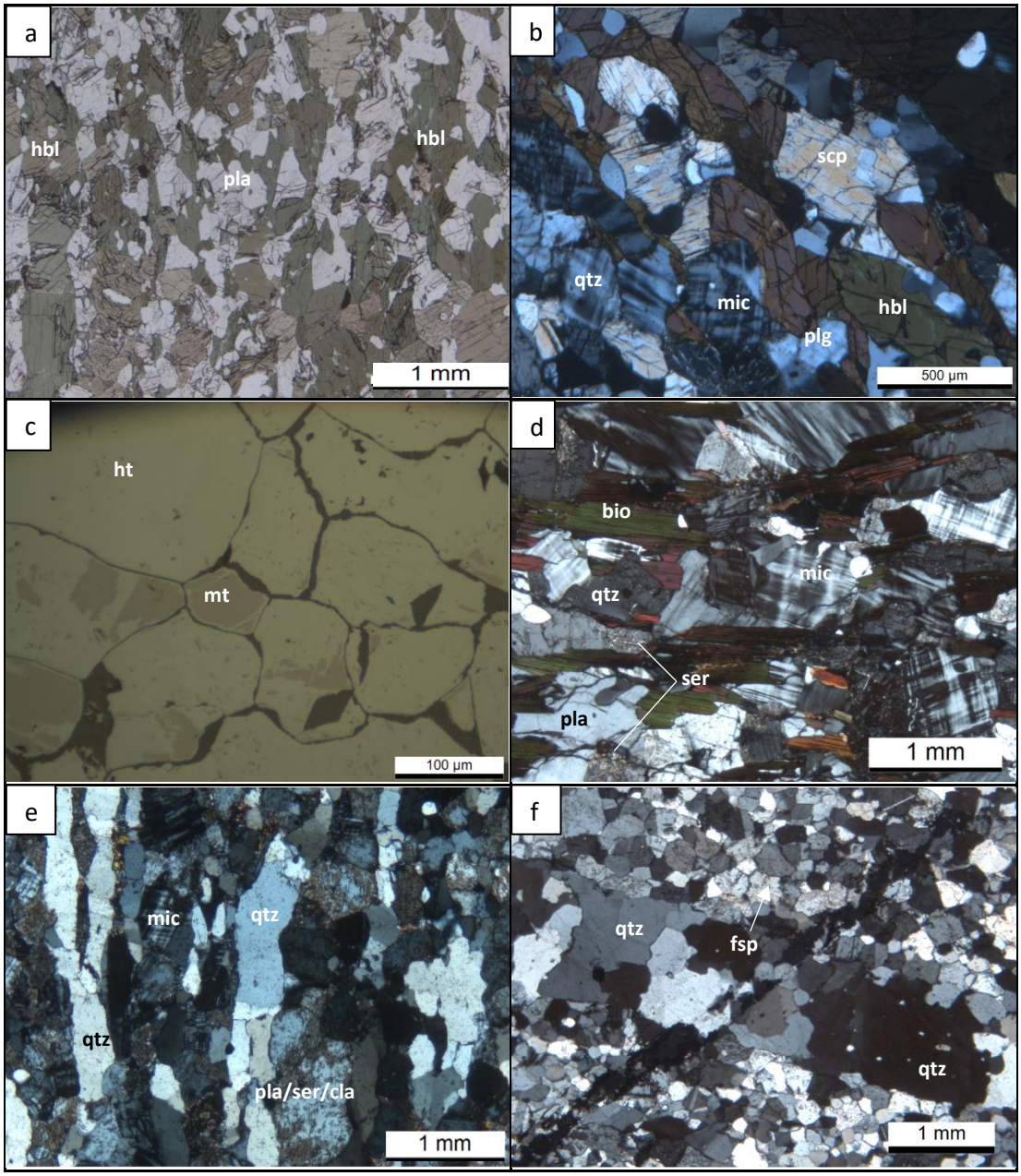


*Figure. 2.5. Photos of thin sections for rock units from Tick Hill. (a) Foliated ($S_1$) amphibolite composed of hornblende (hbl) and plagioclase (pla) (plain-polarized light); (b) Foliated ($S_1$) amphibole-rich calc-silicate with scapolite (scp), hornblende (hbl), plagioclase (pla), microcline (mic) and quartz (qtz) (crossed-polarized light); (c) Hematite (ht)replacing magnetite (mt) in the magnetic calc-silicate sub-unit (reflected light); (d) Foliated ($S_1$) biotite schist composed of quartz, biotite, microcline and plagioclase (crossed-polarized light). The fabric displays annealing textures in which quartz-feldspar grain growth was restricted by biotite grains. Feldspar is partially altered to sericite (ser); (e) Quartz-feldspar mylonite composed of ribbon grains of quartz (qtz), microcline (mic) and plagioclase (pla) that was altered to sericite and clay minerals (crossed-polarized light); (f) Quartz-feldspar mylonite cut by a thin quartz vein (running left to right) that parallels the main mylonitic fabric, and a later fracture filled with opaques (bottom left to upper-right). The quartz displays a granoblastic textures reflecting post-deformational annealing and recovery (crossed-polarized light).*

*Late pegmatite veins*

The gneiss units in the Tick Hill pit were intruded by late-tectonic pegmatite dykes, and the gneissic layering is locally overprinted by pegmatite-like metasomatic alteration zones which developed as rims along late fractures. Although somewhat deformed and locally boudinaged, the pegmatite veins exhibit no penetrative, mylonitic deformation fabrics and they transect the pervasive gneissic layering that characterizes the host rocks.

Late pegmatite veins occur as thin (<0.6 m) dyke-like bodies and preserve a fine- to medium-grained texture of intergrown feldspar-plagioclase and quartz near the margins of the dykes with a core dominated by plagioclase (85-95%) with variable amounts of quartz (<10%), K- feldspar (<5%) and biotite (0-10%). In drill core pegmatite-like veins appear in the footwall of the ore body and are associated with metasomatised zones with a granular texture and diffuse boundaries in which feldspar (~30-40%), quartz (20-30%) and minor biotite (<5%), overprint and replace the underlying metamorphic fabrics. The late-tectonic pegmatite intrusions were strongly affected by later hydrothermal alteration, in which feldspar was replaced by an albite-sericite assemblage.

### *3.2. Deformation sequence in the Tick Hill deposit*

Rocks hosting the Tick Hill deposit were affected by four distinct deformation and metamorphic events: (1) $D_1$ shearing at upper amphibolite to granulite facies metamorphic conditions, (2) $D_2$ upright folding at upper amphibolite facies metamorphic conditions, (3) $D_3$ normal faulting with extensional veining and widespread quartz-feldspar alteration at lower amphibolite to upper greenschist facies, and (4) $D_4$ strike-slip faulting with cataclasite formation along fault planes. Each of the events as seen in the pit and its immediate surroundings, and in drill cores has been described in more detail below.

*$D_1$ events*

The dominant structural element in Tick Hill pit and its immediate surroundings is a well-developed, moderately west-dipping schistose or gneissic layering and associated mineral lineation, which formed during the earliest stages of deformation referred to as $D_1$. This layering consists of an annealed mylonitic fabric with sugary, granoblastic characteristics in quartz-feldspar-rich lithologies (i.e. blasto-mylonites), and has an orientation within the pit that varies from 305/65 (dip direction/dip) to 250/50 (Fig. 2.6a). The layering is a composite tectonic fabric and locally contains isoclinal intrafolial folds, which are best preserved within the calc-silicate unit. Around the hinge zones of the intrafolial folds ($F_1$) an earlier phase of the mylonitic fabric ($S_{1a}$) was folded before being transposed in the dominant fabric ($S_{1b}$). Thus, the main foliation is a composite fabric herein called $S_{1a,b}$ or $S_1$ for short (Fig. 2.7a). $S_1$ contains a well-developed mineral lineation or rodding lineation, $L_{1x}$, which typically pitches steeply to the southwest (251/55, azimuth/plunge, Figs. 2.6a,b). $L_{1x}$ is

defined by the oriented growth of plagioclase aggregates, hornblende and scapolite in calc-silicate and amphibolite units, by biotite and sillimanite in biotite schist, and by quartz-feldspar-rodding in more felsic units and quartzite. $F_1$ intrafolial folds have fold axes that are close to parallel to $L_{1x}$, and sheath-folds have been observed outside the pit.

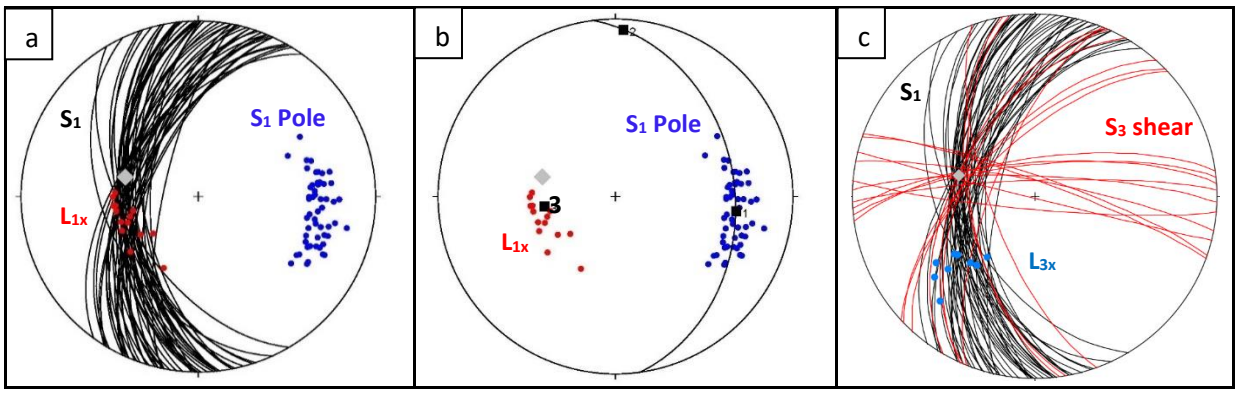


*Figure. 2.6. Lower-hemisphere stereonet of structural elements visible in the pit at Tick Hill. (a) Great circles = $S_1$; blue dots = poles to $S_1$; red dots = $L_{1x}$; grey diamond = long axis of 16.5g/t Au ore envelope. Note that the ore envelope is not parallel to $L_{1x}$. (b) As above. Shown is the best fit great circle through the poles to $S_1$. Note this great circle has a pole (3) that coincides with $L_{1x}$, i.e. the foliation truncation plane responsible for the variations in $S_1$ directions probably formed during $D_1$. (c) Black great circles = $S_1$; red great circles = $S_3$ shear zones and normal faults; blue dots = $L_{3x}$; grey diamond = long axis of 16.5g/t Au ore envelope. Note that the ore envelope is parallel to the intersection lineation between $S_1$ and $S_3$.*

In more quartzo-feldspathic units in the main ore zone, the $S_1$ foliation intensifies to a mm-scale lenticular to laminar fabric characteristic of mylonite (Fig. 2.4i). This fabric has been largely annealed resulting in a granular texture in thin section, characterized by alternating ribbon grains of quartz and plagioclase (Fig. 2.5e). Within the present geometry, trails of rotated boudin blocks of coarse-grained black quartzite layers within calc-silicate, exposed in the north wall of the pit, are consistent with a normal west-down shear sense, but otherwise shear sense indicators (asymmetric clasts, S-C fabrics, shear bands etc.) are lacking.

Across the pit the orientation of $S_1$ varies around two principal groupings: 300/60 and 260/55 (Fig. 2.6). In the western half of the pit, $S_1$ dips to the west-northwest (300/60), whilst in the eastern half of the pit, $S_1$ dips due to the west or south-southwest with $S_1$ steepening from 55 to 70° in the southeast corner of the pit (Fig. 2.3a). $L_{1x}$ does not vary greatly in orientation in either of the two domains and remains more or less constant around 250/55, which is parallel to the intersection line between the various $S_1$ orientations (Fig. 2.6b). An abrupt change in orientation of the $S_1$ foliation occurs in the center of the pit where it can be mapped as a foliation truncation plane, characterized by an intensely foliated biotite-chlorite-schist zone. The foliation truncation plane originated during $D_1$, but was reactivated as a brittle-ductile shear zone during $D_3$ as discussed below. The north to north-northeast trending foliation truncation plane dips ~55° to the west and connects the hanging wall quartzite in the southern wall of the pit to the footwall quartzite in the north (Fig. 2.3a). It more-or-less coincides with the ore zone (Fig. 2.6). Within the open pit, $S_1$ orientations also vary

around quartzite boudins and along 10 m scale northwest-trending shear-band-like high strain zones that locally cross the main foliation (e.g. in the upper benches in the southeast corner of the pit).

Peak-metamorphic conditions in Tick Hill pit were reached during $D_1$ shearing and folding (e.g. Choy, 1994). The grade of metamorphism during $D_1$ reached upper-amphibolite to granulite facies as indicated by the ductile behavior of K-feldspar and plagioclase in sheared quartzo-feldspathic mylonite, intense ductile folding (including sheath folding) in amphibolite, the presence of coarse-grained metamorphic pyroxene in leucocratic segregations within amphibolite, and hornblende-pyroxene and sillimanite assemblages defining the $S_1$-$L_1$ fabrics. In addition, garnet-hornblende-pyroxene-plagioclase-quartz assemblages in amphibolite gneiss were encountered in drill core 800 m north of the pit. The $D_1$ deformation features in Tick Hill correlate with regional $D_1$ deformation events described in the southern MKD (e.g. Blake and Steward 1992; Passchier, 1992; Rutherford, 2000).

Within the pit and surrounding areas numerous quartzo-feldspathic granitic bodies occur that are variably deformed. Many are strongly mylonitic and fine-grained throughout, whereas others preserve less deformed cores with mylonitic rims. The quartzo-feldspathic units were described as the intrusive Tick Hill Complex (Wyborn, 1997) and have been interpreted as granite intrusions that were emplaced syn-tectonically at various times during the development of $S_1$.

*$D_2$ events*

Regional mapping shows that the Tick Hill deposit is situated in the eastern limb of a large (km-scale) synformal, $D_2$ structure (the Tick Hill syncline; Fig. 2.2b) that folds $S_1$ around an upright fold with an axial planar trace that parallels the regional trend of $S_1$. Within the pit no clear $D_2$ structures are visible with the exception of rare open, near-cylindrical similar folds that occur on a 0.1-1 m scale (Fig. 2.7b). Such $F_2$ folds are invariably east-verging with near-horizontal north-trending (020) fold axes, and they contain no clear axial planar fabrics. Metamorphic conditions during $D_2$ are poorly constrained due to the absence of clear $S_2$ fabrics or mineral assemblages, but the highly ductile nature of regional $D_2$ folds, their transposition into the main fabric further west (Laing, 1993) and continued stability of peak assemblages within $D_2$ fold hinge zones suggests that conditions remained high.

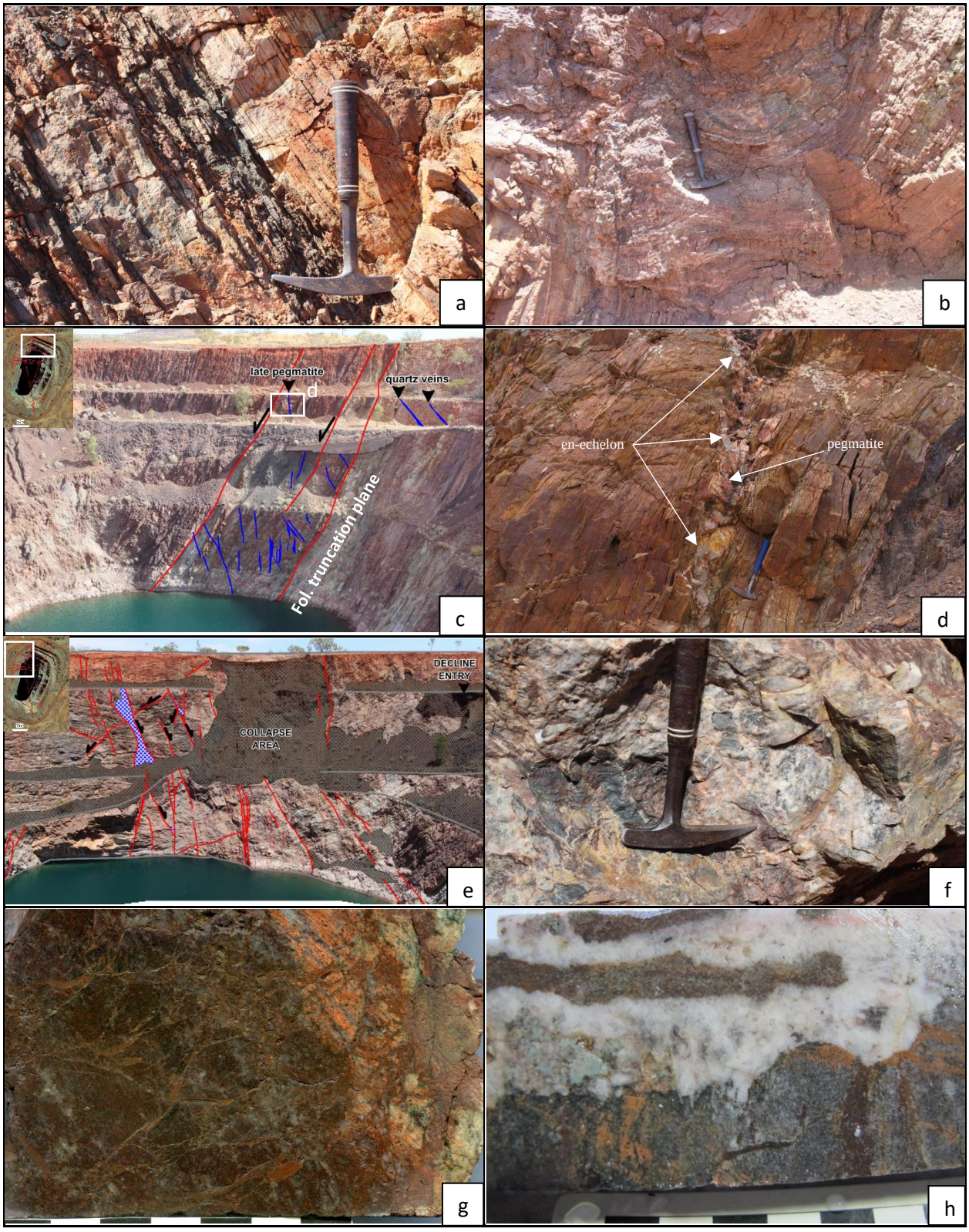


*Figure 2.7. Representative $D_{1\text{-}4}$ structures and alteration textures. (a) $S_1$ fabric in gneissic calc-silicate intercalated with biotite schist bands in the north wall of the pit; (b) $D_2$ up-right folds in the north wall of the pit; (c) North pit wall, showing the $D_1$ foliation plane reactivated as a $D_3$ shear zone (red). En echelon $D_3$ pegmatite and quartz veins (blue) are indicative of sinistral-normal movement on the shear zone during $D_3$; (d) Close-up of syn-$D_3$ pegmatite containing en-echelon quartz veins in (c) that indicate a normal shear sense; (e) East-trending, $D_3$ normal faults (red), some with breccia (blue) in the northwest corner of the pit; (f) $D_3$ brecciated and altered calcsilicate gneiss with trace sulphides derived from underground workings; (g) High-*

*grade calc-silicate breccia in the ore zone, which is associated with $D_3$ sheeted veins and quartz-feldspar-chlorite-hematite alteration; (h) $D_4$ veins with calc-silicate breccia fragments consisting of quartz, carbonate and green clay minerals that over print the late $D_3$ red rock alteration.*

*$D_3$ events*

$D_3$ in the Tick Hill pit is characterized by a network of fault zones and associated fractures and veins that accommodated normal movements and facilitated retrograde alteration (Figs. 2.7c-e). The $S_1$ foliation is locally reactivated as, or truncated by $D_3$ fault zones, that are characterized by a micaceous foliation and the alignment of fine-grained chlorite (after biotite) to define $L_{3x}$ (most clearly observed in the northern wall of the pit). This lineation pitches shallowly to moderately south-southwest (~230/40, Fig. 2.6c), and is locally paralleled by quartz striations. $D_3$ fault planes are associated with damage zones including breccia zones and quartz veins, some of which are arranged in an en-echelon fashion (Figs. 2.7c,d) consistent with a sinistral-normal sense of movement. The most conspicuous $D_3$ shear is exposed in the northern wall of the pit as a biotite-chlorite schist zone that parallels the $D_1$ foliation truncation plane passing through the center of the pit. This fault zone coincides with the ore zone. $D_3$ fault zones also developed along the margins of the quartzite units and a major fault truncates the hanging wall quartzite in the southern wall of the pit (Fig. 2.3a).

A series of parallel, east-trending, steeply (mostly north) dipping, normal faults (Figs. 2.3a, 2.6c, 2.7e) are prominently developed in the northwest corner of the pit. These faults mostly do not cross the pit but appear to merge with the north-northeast-trending $D_3$ faults in the center of the pit, including the main $D_3$ fault that parallels the $D_1$ foliation truncation plane (Fig. 2.3a). The east-trending faults display dm- to m-wide, quartz-feldspar alteration haloes or rims developed on either side of individual faults, and associated albite-epidote-hematite veins.

$D_3$ faulting involved widespread fracturing, veining, breccia formation and quartz-feldspar alteration visible in outcrop and in drill core. These features are concentrated in the strongly silicified core of the deposit, and the $D_3$ fracturing, at least in part overprints earlier silicification. Fracture sets include thin (< 2 mm wide) grey quartz veins that trend between 80-100° and that occur as bundles of partings along the $S_1$ mylonite fabric, especially in the quartz-feldspar mylonite, and drill intersections suggest that breccia is commonly associated with the sheeted veins in the lower levels of the high-grade ore zone (Figs. 2.3b; 2.7f,g).

Fracture sets also include northeast trending faults (~030) that display sinistral displacements in drill core and are associated with albite-hematite altered quartz veins, and north- and east-trending cataclastic shatter zones best developed in silicified quartzite and schist. $D_3$ fractures are commonly highlighted by pink and red feldspar alteration, which also forms the matrix to shatter zones along fractures. In the ore zone (the "galahstone"), these fracture sets merge into a continuous network and many of the fractures and associated quartz veins contain visible gold. Steep east-trending fracture zones are present in all drill cores through the ore zone, and they are particularly common in gold-bearing zones. In some drill cores the fracture zones widen

to several 10s of cm where they are characterized by chaotic fabrics (poor core recovery) and breccia. $D_3$ fracture zones coincide with widespread quartz-feldspar-chlorite-hematite alteration as well as locally developed carbonate alteration.

Several drill cores preserve late-stage, coarse-grained quartz-feldspar veins, which resemble the metasomatic alteration rims that decorate $D_3$ fractures and veins. These late tectonic quartz-feldspar zones have been interpreted as syn-$D_3$ metasomatic overgrowths.

*$D_4$ events*

$D_4$ structures represent the latest phase of deformation recorded in the Tick Hill pit. On the scale of the pit, $D_4$ involved the formation of brittle east-northeast-trending and steeply north-dipping faults (Fig. 2.3a) that formed in combination with steep northwest-trending secondary faults. The main east-northeast-trending fault has an apparent dextral displacement. $D_4$ faults displace the quartzite units and are associated with cataclasite formation and chlorite-hematite-goethite alteration along slicken-sided fracture zones as well as open-space carbonate fill. In drill core, $D_4$ structures include late-stage fractures and cataclasite zones with quartz-carbonate-clay fill and associated clay alteration haloes, which overprint $D_3$ fractures and veins (Fig. 2.7h).

## 4. Gold mineralization and alteration at Tick Hill deposit

As mentioned in the introduction earlier workers at Tick Hill noted the problem that gold seemed to have a relationship to both old ($D_1$) and young ($D_3$) structures (e.g. Choy, 1994; Tedman-Jones, 2001). Gold inclusions in peak-metamorphic minerals, an alignment of gold with the $S_1$ fabric and a spatial association with syn-$D_1$ silicified deformation zones were cited as evidence for early gold (e.g. Choy, 1994). A spatial association with late-tectonic laminar quartz veins and associated chlorite-albite-hematite alteration, and the presence of gold along $D_3$ fractures and breccia zones were cited as evidence for a $D_3$ origin (e.g. Tedman-Jones, 2001). What follows is a description of gold distribution patterns and associated mineral assemblages in relation to the earlier and later structures. An in depth discussion of the potential genesis of the ore body is provided in the discussion.

### *4.1. Ore body geometry and associated metal distribution*

The ore body geometry as defined by the 1 g/t ore envelope for the Tick Hill deposit is carrot-shaped and tapers down to a vertical depth of 240 m (MIM 1993, 2000; Tedman-Jones, 2001). The ore body dips ~55º to the west, i.e. parallel to $S_1$, and has a linear high-grade (i.e. 16.5 g/t) core that plunges 55° to 285 (Fig. 2.6). With increased depth, the strike extent of the ore zone decreases and in the two lowest mine levels (130 mRL and 117 mRL; e.g., Fig. 2.3b), the ore trend switches abruptly from north-northeast (Fig. 2.3a) to east

and the ore zone narrows to several meter-wide chlorite-hematite-carbonate breccia veins (Fig. 2.3b, Tedman-Jones, 2001).

The geochemical surface expression of the Tick Hill gold anomaly (> 0.1ppm) was about 160 × 30 m and coincided with a pre-mining, north-northeast-trending, 210 × 50m magnetic low (Nano et al., 2000, Fig. 2.8). The location of the gold anomaly that runs across the pit overlaps with a strongly $D_3$ fractured and hematite-altered zone in the immediate hanging wall of the $D_1$ foliation truncation plane that was reactivated as a $D_3$ shear zone (Figs. 2.3a, 2.6b). The plunge of the high-grade core of the ore body coincides with the intersection lineation between the north-northeast- and east-trending $D_3$ faults and the intersection lineation between the $D_3$ faults and the $S_1$ foliation planes as measured in the pit. The plunge of the high-grade core is also close in orientation to the measured $L_{1x}$ mineral lineation, which is somewhat variable in orientation (Figs. 2.3a, 2.6c). The low grade (i.e. 0.1 g/t) ore envelope coincides with areas where east-trending $D_3$ fractures and breccia zones are most prominent, and extends outside the pit along some of the more prominent east-trending $D_3$ fracture zones.

Gold mineralization is largely confined to the strongly altered quartz-feldspar mylonite sub-unit and adjacent biotite schist, calcsilicate, and hanging wall quartzite (Fig. 2.3). The historical assay data shows that the boundaries to the mineralization are sharp as grades drop abruptly away from the $D_{1-2}$ silificied and $D_3$ altered fracture zones. Gold occurs almost exclusively as disseminated grains of free gold up to 0.5 mm in size with Au/Ag ratios of >100.

In drill cores and thin sections, gold can be commonly seen as an alignment of coarse grains that parallel the dominant mylonitic $S_1$ fabric. Gold grains also commonly occur associated with thin laminar quartz veins of $D_3$ origin, which either occur along the $S_1$ mylonitic foliation or along steep east-trending fractures. Mineralization shows a spatial relationship with $D_3$ alteration haloes near post-tectonic coarse-grained quartz-feldspar dykes, and fine gold grains typically occur near patches of chlorite, albite and hematite. The east-trending quartz-feldspar veins are locally associated with breccia zones, which in drill core are most prominent at depth in the immediate footwall of high-grade ore zones (Figs. 2.7f,g). At shallower levels where breccia is less common, high-grade mineralization is concentrated in areas of intense laminar $D_3$ veining (Figs. 2.4i, 2.9a,c).

The quartzo-feldspathic mylonite is locally extremely gold-rich (e.g. up to 3209 ppm @ 0.5 m in DH TH014), and gold grains locally display a characteristic granoblastic texture. Within the high-grade ore zones, gold grains commonly display bimodal grainsize distributions with irregularly shaped larger grains surrounded by a halo of finer grains (e.g. Choy, 1994, Figs. 2.9d,f). A few of these finer grains contain small amounts of Ag (< 5.3 wt.%) and Cu (< 2 wt.%). Coarse-grained gold is commonly enclosed within recrystallized quartz, with quartz appearing as a metamorphic moat around the gold. Gold also occurs along the grain boundaries

between quartz and feldspar grains (Fig. 2.9b). Within calc-silicate units, gold is locally enclosed within granoblastic, hornblende, scapolite and pyroxene grains that are aligned in the peak-metamorphic $S_1$ fabric (Figs. 2.9d-e). Fine-grained gold occurs either as haloes near larger gold grains or as trails associated with strongly silicified zones and alteration minerals that included bismuth selenides and sulfides (Table 2.2). In general, the sulfide content in the mineralized quartz-feldspar mylonite unit is less than in the other units, and the abundance of sulfides increases towards the footwall of the deposit.

The high-grade core of the Tick Hill deposit shows only minor enrichment in other metals, and sulfides. Available assay data for a restricted number of elements (Cu, Co, Ni, Pb, Zn, As, Fe, Mn) from exploration holes drilled in the 1990s (MIM, 2000) indicate that with few exceptions, on a meter-scale, gold values show no correlation with any of the other metals. On a scale of the entire deposit, a general enrichment in Cu (> 100 ppm), Co (> 40 ppm), S, As, and Bi has been suggested for the immediate footwall of the ore zone (Nano 1999; Tedman-Jones 2001), with minor Co enrichment (> 40 ppm) partly overlapping with the 1 g/t Au envelope. Cu values reach up to several 1000 ppm in the footwall to the ore zone and can be linked to chalcopyrite-pyrite and minor bornite-pyrrhotite mineralization, which is possibly also responsible for an induced polarization anomaly that was observed over the Tick Hill ore body (Nano, 1999). Cu values are rarely high in the ore zone itself. At a larger scale, it is clear that Cu and Co anomalies are not just restricted to the vicinity of the ore zone, but also occur in the hanging wall of the ore zone, where Cu values locally reach 100's ppm away from mineralization and alteration (Fig. 2.10). In general Cu shows moderate to strong correlations with Co and Ni and a spatial relationship with amphibole-rich lithologies.

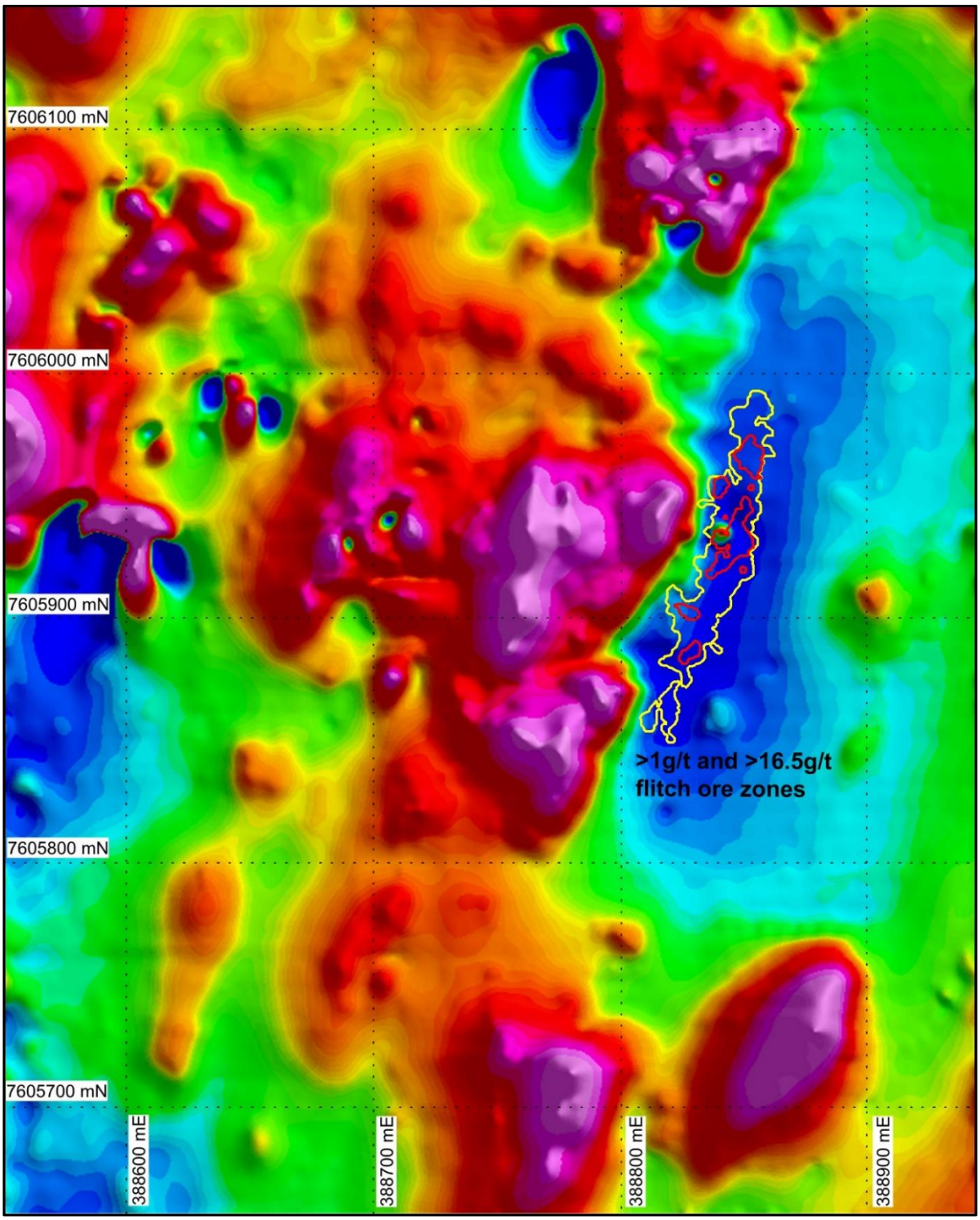


*Figure 2.8. Ground magnetic map of the Tick Hill area, overlain with Au grade contours, illustrating the coincidence of gold mineralization with the area of magnetic depletion (Nano et al., 2000).*

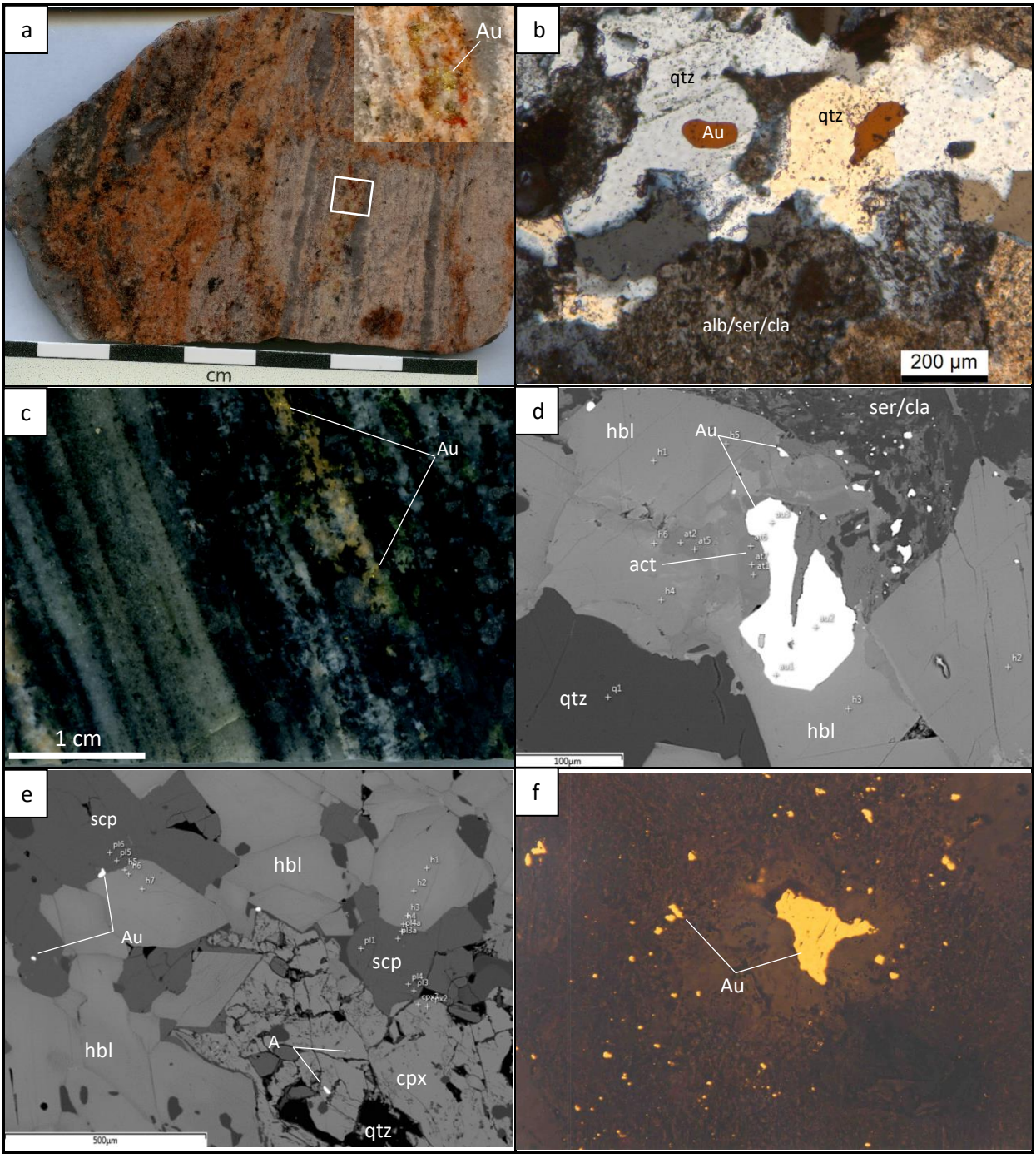


*Figure 2.9. Examples of textures associated with gold mineralization. (a) Gold-rich metasomatized quartz-feldspar mylonite, a close-up of the white box is shown in the top right; (b) close-up of coarse-grained gold grains in (a). Gold is commonly contained within quartz or surrounded by a moat of quartz in recrystallised quartzo-feldspathic gneiss in which albite is replaced by late-$D_3$ sericite and clay minerals; (c) Gold mineralization concentrated along feldspar-rich selvages in strongly foliated amphibole-rich calc-silicate; (d). A SEM image showing coarse-grained gold within peak-metamorphic ($D_1$) hornblende, while fine-grained gold occurs along grain boundaries where it is associated with sericite (ser) and clay (cla) alteration (after feldspar); (e) A SEM image showing gold inclusions hosted within peak-metamorphic clinopyroxene (cpx) and scapolite (scp) from amphibole-rich calc-silicate; (f) Microphotograph showing a coarse grain of gold with a halo of finer gold grains suggesting local dissolution and remobilisation of early stage gold (image after Choy, 1994).*

### *4.2. The spatial distribution of the alteration halo around gold mineralization*

The Tick Hill deposit is associated with two periods of alteration: a first that occurred at high temperatures during $D_1$, and a second that occurred at lower temperatures during $D_3$. Early high temperature alteration involved the emplacement of gold that was incorporated in hornblende and diopside grains aligned in the $S_1$ fabric. Evidence for this early event is only partly preserved, because of the intensity of the later stages of hydrothermal overprints during $D_3$, and the exact spatial distribution of the early alteration halo is uncertain.

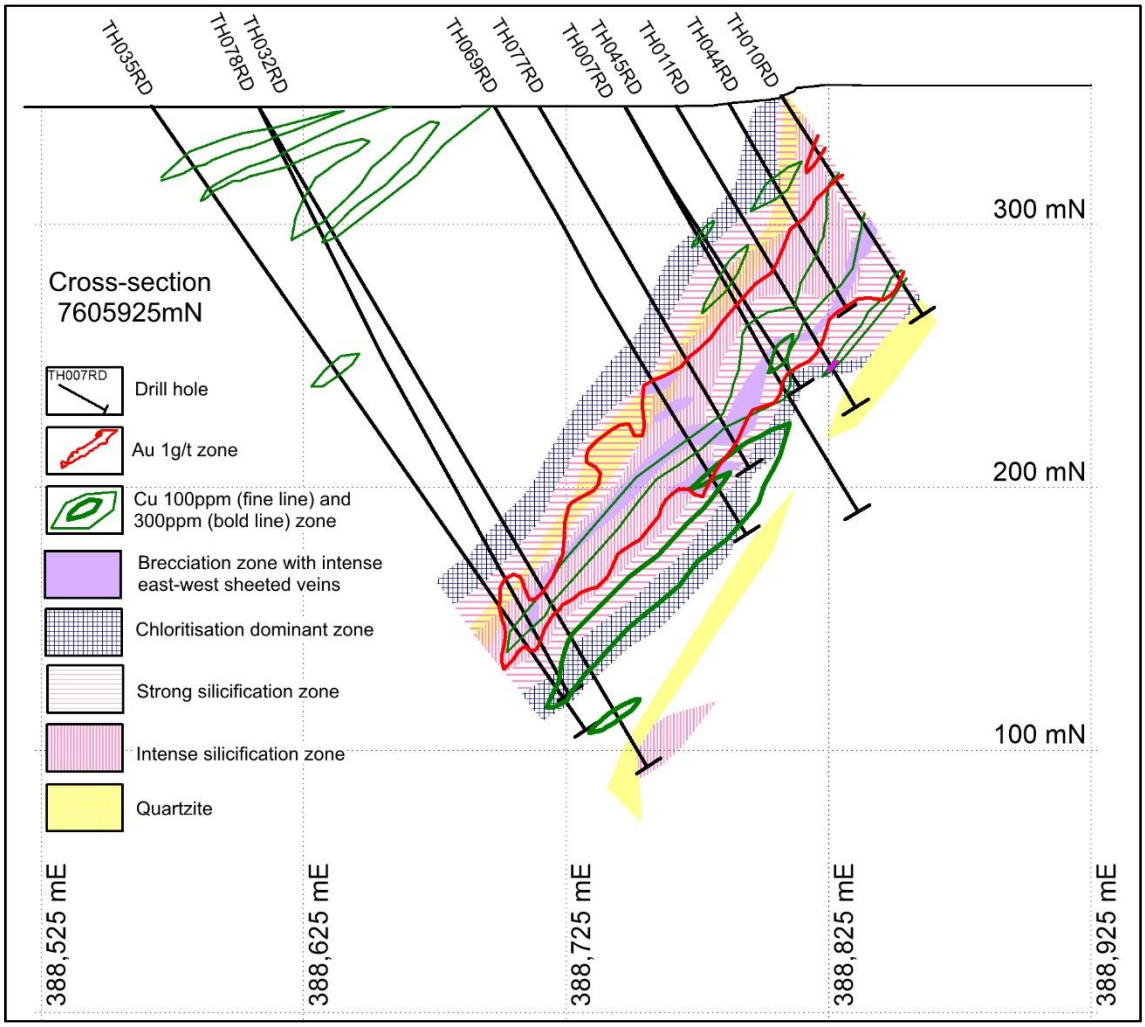


*Figure 2.10. Cross-section 7605925mN showing the spatial relationship between various alteration zones, brecciation, 100-300 ppm Cu zone and the 1g/t ore envelope at Tick Hill based on core logging and assay data.*

The early alteration event is characterized by intense silicification and magnetite alteration (e.g. Fig. 2.4c; Appendix 6A, page 385) that is most evident within the hanging wall quartzite unit. Within the ore zone, syn-$D_1$ silicification was intense and involved the growth of quartz at the expense of other silicate phases (Fig. 2.11b), which now occur as inclusion trails in quartz. Early magnetite alteration was largely destroyed by the lower temperature $D_3$ hydrothermal overprint during which magnetite was replaced by $D_3$ hematite.

Gold grades in drill core today display a negative correlation with magnetic susceptibility, and this effect is visible on a larger scale by the presence of an aeromagnetic low that coincides with the ore zone and the $D_3$ alteration halo (Fig. 2.8).

The younger $D_3$ alteration events resulted in the formation of a clear low- to moderate-temperature alteration zone that is about 100 m in diameter, which developed during $D_3$ and overprinted the earlier high temperature alteration assemblages as well as the $D_1$ peak metamorphic mineral assemblages and associated structures (Figs. 2.3, 2.10). This later alteration is most prominently developed in the ore zone and hanging wall rocks to the ore zone above the $S_{1\text{-}3}$ foliation truncation plane, whilst the footwall rocks to that surface are significantly less altered (Geological Survey of Queensland, 2015).

The lower temperature alteration assemblages vary with rock type and display a zonal pattern, with most intense alteration occurring along $D_3$ fracture zones and associated breccia. From the proximal mineralization outward, the alteration zonation includes (Fig. 2.10): (1) intense to (2) strong silicification and associated growth of abite-hematite-chlorite-epidote-sericite-actinolite/hornblende-oligoclase, surrounded by (3) a shell characterized by chlorite and epidote, and (4) an extensive zone with clay alteration. Zonal boundaries are gradual with localized overlaps in alteration assemblages, whilst late clay alteration occurs throughout.

The most extensive expression of low-temperature alteration in drill core includes the presence of smectite and illite with minor hematite and quartz in veins, and as replacement of feldspar. This type of alteration typically occurs in association with quartz-feldspar veins in the hanging wall calc-silicate and amphibolite units. Intense clay alteration is also well developed within the more reactive felsic units and biotite schist in the immediate footwall to gold mineralization (Geological Survey of Queensland, 2015). The clay minerals occured throughout most drill holes, tens of meters from the mineralization zones (e.g. Appendix 1, Geological Survey of Queensland, 2015).

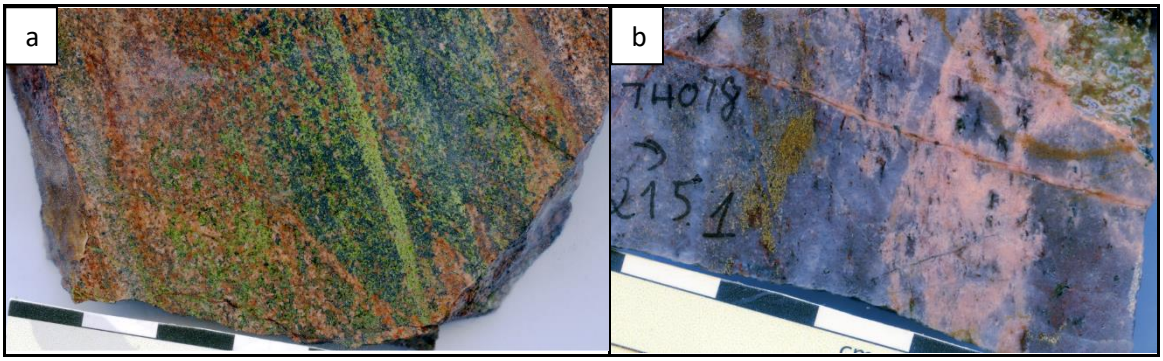


*Figure 2.11. Examples alteration from Tick Hill deposit. (a) A cm-scale image of chlorite-epidote alteration in the hanging wall to mineralization; (b) A cm-scale image of the $D_{1\text{-}2}$ silicification zone, with relic biotite, overprinted by $D_3$ pink feldspar-quartz alteration and gold mineralization (gold is found in the sheeted veins in association with chlorite and feldspar at the center of the image).*

On the hanging wall side and closer to mineralization, chlorite-epidote alteration overprints the older quartz-magnetite alteration, especially along the contact zone between the calc-silicate unit and hanging wall quartzite, and near the base of the hanging wall quartzite unit (Fig. 2.11a). The immediate halo to the ore zone is characterized by strong silicification that is spatially associated with patches and/or veinlets of pink albite and chlorite-epidote-actinolite-hematite-sericite-calcite alteration, as well as gold and minor sulfides. The alteration is pervasive and is concentrated in veins, along fracture zones and as disseminations along microfracture networks. In this zone, primary feldspar was replaced by sericite, albite and clay minerals (illite, smectite), whilst magnetite and ilmenite were altered to hematite and leucoxene, and chlorite replaced biotite.

Within the high-grade ore zone, intense silicification affected the quartz-feldspar mylonite and biotite-rich schist (Fig. 2.11b). Here, pervasive silicification with quartz growth across the mylonitic fabric occurred early (i.e. pre- or early-$D_3$), with later silicification linked to the emplacement of thin quartz veins (sub-) parallel to the $S_1$ foliation, and the growth of quartz in alteration haloes near quartz-feldspar veins and pegmatite dykes. Other alteration minerals in this zone include albite, oligioclase, K-feldspar, hornblende, actinolite, chlorite, epidote, sericite, calcite, hematite, and leucoxene.

Carbonate alteration generally occurs as a late late-$D_3$ and $D_4$ fracture fill. In the mineralized zone, calcite locally occurs as secondary growth along sheeted quartz veins and east-trending fractures, but carbonate growth is not pervasive. However, in the keel of the deposit in the lower levels of the mine, gold was mined from east-trending breccia veins that were reported to contain chlorite-hematite-carbonate in the matrix (Tedman-Jones, 2001), i.e. at depth carbonate growth may have been more abundant and it occurred in associated with gold, although we could not confirm this in drill core.

### *4.3. Paragenetic sequence*

Most hydrothermal alteration minerals associated with gold mineralization formed during $D_3$. However, there is clear textural evidence that gold was present during $D_1$ peak metamorphism when the main gneissic fabric formed and an early stage of high temperature alteration occurred (Table 2.1. The main minerals that characterize early, high temperature alteration are magnetite and quartz, which are best preserved in the hanging wall quartzite unit, where quartz and magnetite largely replaced biotite, feldspar, and in places amphibole (e.g. Geological Survey of Queensland, 2015), which are now only visible as trails of largely resorbed grains aligned along $S_1$ and included in granoblastic quartz. The magnetite content in the hanging wall quartzite increases upwards and grades into a near-massive magnetite zone towards the upper contact of the quartzite, where magnetite is aligned with $S_1$ and inter-grown with syn-$D_1$ high-temperature minerals including scapolite and hornblende, suggesting that much of it formed pre- or syn-$D_1$ (Table 2.1). Considering that the early magnetite-quartz alteration is prominent in the hanging wall of the high-grade ore zone, and magnetite within the ore zone itself was largely replaced by $D_3$ hematite (Fig. 2.8), it is likely that early magnetite alteration was associated with deposition of early gold.

The best evidence for early gold mineralization can be found in mineralized amphibolite-rich, calc-silicate gneiss horizons, where granoblastic gold inclusions occur in peak-metamorphic scapolite, hornblende and diopside grains that were unaffected by later retrograde alteration (Figs. 2.9d-e). There are no obvious micro-fractures in the scapolite, clinopyroxene or hornblende grains that could indicate later remobilization of gold, and the presence of these inclusions strongly suggests that gold was present when the $S_1$ fabric formed. The presence of early gold is further supported by its bimodal grainsize distribution in some high-grade ore zones, where coarse gold grains that are typically aligned in the $S_1$ fabric and surrounded by a halo of fine gold (Figs. 2.9d,f; Choy, 1994).

Emplacement of early gold may have been associated with the deposition of sulfides. Texturally early $D_1$ chalcopyrite has been observed as inclusions inside amphibole, which itself occurs as inclusions inside coarse-grained, peak-metamorphic, almandine garnet (e.g. in drill core TH99, 800 m north of Tick Hill). Away from the main ore zone, chalcopyrite and pyrite are relatively common in amphibolite gneiss, where the sulfides occur along $S_1$ foliation traces. Thus, a first stage of gold mineralization occurred in association with the peak-metamorphic assemblage and an early stage of magnetite-quartz alteration when chalcopyrite was present within the system (Table 2.1).

The most obvious alteration assemblages visible in the Tick Hill pit today formed during $D_3$ and $D_4$, and involved six hydrothermal stages (Table 2.2). During stage 1, magnetite-bearing feldspar veins were emplaced associated with the formation of an alteration assemblage (stage 1) that included quartz-albite (±oligioclase)-hornblende-magnetite-hematite (±leucoxene). This was followed by at least three stages during which gold was either introduced or remobilized, with hematite and chlorite being the most characteristic alteration minerals in outcrop. Stage 2 coincided with the main period of gold enrichment, and involved quartz-feldspar veining and alteration characterized by the growth of quartz-albite-actinolite-chlorite$_1$-hematite (±leucoxene) progressing into stage 3 with the growth of K-feldspar-sericite-chlorite$_2$-epidote-hematite (early stage 3) followed by hematite, smectite and illite (late stage 3). Stage 4 is characterized by minor calcite veining, late chlorite$_3$ growth and the remobilization of some gold along fractures. Stage 5 events postdated mineralization and included late-$D_3$, pale pink quartz-albite flooding and the renewed growth of magnetite along isolated fractures. During later $D_4$ events additional quartz-carbonate-clay alteration (stage 6) occurred along late faults, with no evidence that gold was remobilized. The paragenetic sequence and mineral assemblages that formed during each of these six stages are discussed in more detail below and presented in Table 2.2.

The early-$D_3$ emplacement of ***stage 1*** feldspar veins marked the onset of younger hydrothermal alteration events that predated the introduction of new gold during $D_3$, or the re-mobilization of early gold that had formed during $D_1$. Most veins of this type are steep and have an east trend (Fig. 2.12a), and they contain magnetite and titanite. They represent the earliest set of veins that form part of the family of laminar, sheeted veins that characterize the ore zone. They are common in the hanging wall sequence, and their occurrence in

the footwall sequences is uncertain, due to a paucity of available drill core. Vein emplacement was associated with the formation of a mineral assemblage (stage 1) that included quartz-albite-oligioclase-hornblende-magnetite-hematite (±leucoxene). Intense albite alteration characterized stage 1 and occurred with the formation of oligoclase, hematite and hornblende. Stage 1 magnesio-hornblende (Mg/Mg+Fe = ~0.6, minor $Na_2O$, $K_2O$, Cl, and $TiO_2$) is blue-green in colour (Fig. 2.13a), and either replaces older $D_1$ hornblende, or occurs as clots overgrowing the dominant fabric.

During ***stage 2***, numerous feldspar-rich veins were emplaced that either contained gold, or that were associated with alteration haloes that contained gold (Figs. 2.12b-d). These veins included thin (< 1 mm), east-trending, laminar veins, and north-trending veins that can be up to 10 cm wide and parallel the $S_1$ foliation. The stage 2 veins were best developed as feldspar-filled fractures within the silicified biotite-rich schist, in quartz-feldspar mylonite and in the hanging wall quartzite (Figs. 2.12b-c). Stage 2 veins consist of pale pink to dark pink feldspar and quartz. The pale pink feldspar is commonly albite with lesser oligioclase, while the darker pink feldspar is either albite or oligoclase with abundant fine-grained hematite inclusions. Overprinting relationships between veins in some drill cores suggest that stage 2 veining commenced with feldspar-rich veins and continued with the emplacement of progressively more silica-rich veins.

Stage 2 veins are associated with extensive feldspar alteration haloes that emanate from the veins, and overgrow and replace the older $S_1$ fabric (Fig. 2.11b). Alteration textures vary in intensity and include: (a) albite (±oligoclase) replacement with minor quartz that obliterated the older fabric, (b) albite-quartz alteration along thin laminates that generally parallel the $S_1$ fabric, and (c) replacement alteration along networks of fine fractures that resulted in a spotted and veined alteration texture (Fig. 2.12c). Most gold observed in thin sections occurs in spatial association or is inter-grown with stage 2 alteration assemblages, and it commonly occurs as inclusions within granoblastic, grey quartz grains (Fig. 2.9b). The mineralization was associated with the growth of albite-hematite-actinolite-chlorite$_1$ and later K-feldspar-sericite (Figs. 2.13a-f). Intense albite alteration with oligoclase occurred early during stage 2, and became weaker towards stage 3, as K-feldspar started to develop. In general, K-feldspar formed after albite, and locally appears as reaction rims on albite grains (Fig. 2.13d). K-feldspar is commonly hematite-dusted, and together with hematite-dusted albite forms the red-pink feldspar alteration that characterizes stage 2 alteration zones.

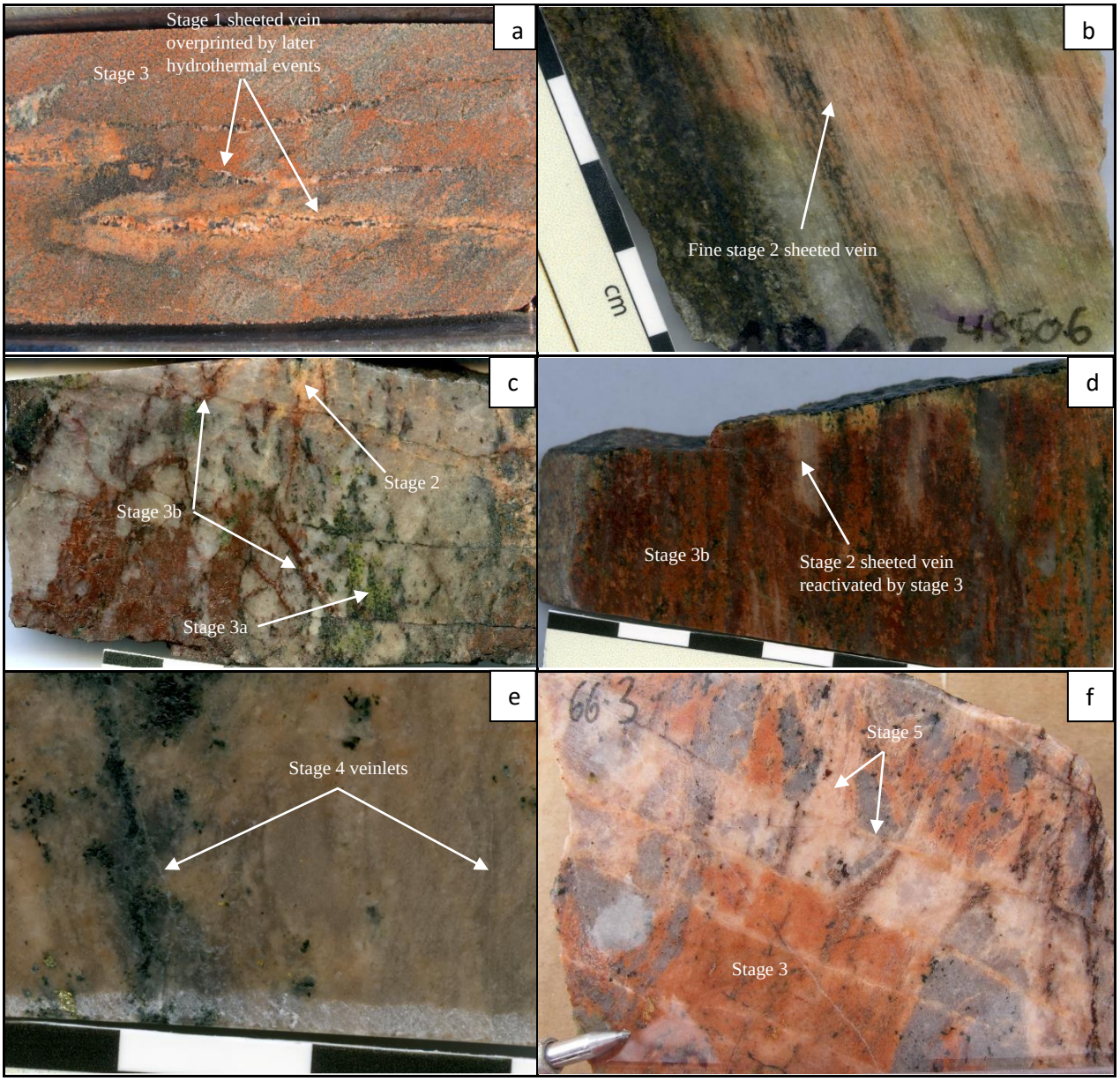


*Figure 2.12. Examples of alteration assemblages in drill core from the high-grade ore zone, reflecting the paragenetic stages recognised in Tick Hill. (a) Stage 1 east-trending sheeted veins comprised of quartz, feldspar and magnetite, which were overprinted by stage 3 red rock alteration (RRA). (b) Stage 2, east-trending, finely laminated, sheeted veinlets and associated pink feldspar-quartz alteration haloes overprinting the $S_1$ fabric. Note that many of the sheeted veins parallel the mylontic fabric and resemble quartz-ribbon grains, thus masking their abundance. (c) High-grade gold mineralization in intensely silicified biotite schist, associated with east-trending, stage 2 sheeted quartz-feldspar veins (pink) overprinted by stage 3a chlorite-epidote and stage 3b hematite-rich alteration. (d). Stage 3 RRA pervasively altered silicified biotite schist with stage 2 sheeted veins. (e) Stage 4 veinlets of calcite overprinting earlier amphibole and quartz-feldspar alteration. (f) Stage 5 light pink feldspar reactivated the stage 1 and 2 sheeted veins and over printed stage 3 RRA.*

Stage 2 sericite alteration is common in the mineralized zone and replaced earlier albite and oligoclase (Figs. 2.9b, 2.13a). The intensity of sericite alteration varies with proximity to stage 2 veining and is commonly associated with hematite, fine-grained gold, and minor $pyrite_1$ and chalcopyrite. Hematite formed as fine inclusions in feldspar, as grains replacing magnetite and as separate grains (Fig. 2.13g). Hematite commonly

contains some titanium and it is intergrown with leucoxene. Stage 2 chlorite$_1$ replaced peak-metamorphic $D_{1-2}$ biotite (Figs. 2.13b,c), and consists of relatively Fe-rich (~30-35% $FeO_{total}$) ripidolite to picnochlorite. It is characterized by a relatively high $Al_2O_3$ (> 18.5 wt.%) and minor MnO (0.1-1.3 wt.%) and $TiO_2$ (< 0.2 wt.%) contents. Stage 2 actinolite is restricted to retrograde rims of stage 1 hornblende (Fig. 2.13a).

Within the ore zone, sulfide minerals are relatively rare, and they typically exhibit irregular, resorbed grain shapes of intergrown pyrite, pyrrhotite and chalcopyrite, with rare bornite, chalcocite, arsenopyrite, and unspecified Ni-Co-Cu-(±Fe) sulfides (possibly (Fe-) Carrollite) that formed during stage 2. Apart from the sulfides, fine gold grains are commonly associated with stage 2 and stage 3 Bi-selenides (e.g. Guanajuatite, $Bi_2Se_3$), which in many places are more common than sulfide. Where pyrite is present, texturally early stage 2 pyrite$_1$ is commonly Ni-rich, and overgrown by late stage 2 Se (±As)-rich pyrite$_2$ (stage 2) and late stage 2 and stage 3 Se-rich pyrrhotite.

*Table 2.1. Peak-metamorphic mineral assemblages in major rock units.*

| *Minerals* | *$D_{1-2}$ Biotite schist* | *$D_{1-2}$ Calc-silicate* | *$D_{1-2}$ Amphibolite* | *$D_{1-2}$ Qtz-fsp mylonite* |
|---|---|---|---|---|
| *Sillimanite* | | | | |
| *Biotite* | | | | |
| *Amphibole* | | | | |
| *Plagioclase* | | | | |
| *K-feldspar* | | | | |
| *Quartz* | | | | |
| *Diopside* | | | | |
| *Scapolite* | | | | |
| *Garnet (Almandine > Pyrope > Grossular)* | | | | |
| *Apatite* | | | | |
| *Magnetite* | | | | |
| *Ilmenite (±Mn)* | | | | |
| *Gold (inclusion)* | | | | |
| *Chalcopyrite* | | | | |
| *Pyrite* | | | | |

*Quantity: Dominant* — *Minor*

*Table 2.2. Retrograde mineral paragenesis for high-grade ore zones at Tick Hill*

| *Minerals/ Deformation events* | *$D_3$* | | | | | *$D_4$* |
|---|---|---|---|---|---|---|
| | *Stage 1* | *Stage 2* | *Stage 3* | *Stage 4* | *Stage 5* | *Stage 6* |
| *Quartz* | | | | | | |
| *Albite* | | | | | | |
| *Oligoclase* | | | | | | |
| *K-feldspar* | | | | | | |
| *Hornblende* | | | | | | |
| *Actinolite* | | | | | | |
| *$Chlorite_1$* | | | | | | |
| *$Chlorite_2$* | | | | | | |
| *$Chlorite_3$* | | | | | | |
| *Epidote* | | | | | | |
| *Sericite* | | | | | | |
| *Clay minerals (smectite-illite)* | | | | | | |
| *Calcite* | | | | | | |
| *Magnetite* | | | | | | |
| *Hematite* | | | | | | |
| *Leucoxene* | | | | | | |
| *Gold (Cg matrix)* | | | | | | |
| *Gold (Fg matrix)* | | | | | | |
| *Gold (Fractures)* | | | | | | |
| *Chalcopyrite* | | | | | | |
| *Bornite* | | | | | | |
| (Fe-) Carrollite *? (Ni-Co-Cu-S±Fe)* | | | | | | |
| *Pyrrhotite* | | | | | | |
| *$Pyrite_1$* | | | | | | |
| *$Pyrite_2$* | | | | | | |
| *Pyrite (undifferentiated)* | | | | | | |
| *Guanajuatite, $Bi_2Se_3$* | | | | | | |
| *Junoite, $Pb_3Cu_2Bi_8(S,Se)_{16}$* | | | | | | |
| *Cerromojonite; $CuPbBiSe_3$* | | | | | | |
| *Molybdomenite; $PbSeO_3$* | | | | | | |

*Quantity: Dominant* — *Trace*

***Stage 3*** alteration is a progression of stage 2 and involved strong green-blue $chlorite_2$-epidote alteration (stage 3a, Fig. 2.12c) followed by pervasive clay-hematite alteration that overprints the earlier assemblages (stage 3b, Figs. 2.12c-d). The intensity of this alteration as seen in drill core is related to the fracture density and the lithological composition, and, more specifically, the amount of primary ($D_{1-2}$ and early $D_3$) plagioclase and magnetite. Stage 3 alteration is associated with gold, which could have been either remobilized from earlier

gold or newly introduced. Alteration minerals include illite and smectite (Appendix 1; Geological Survey of Queensland, 2015), hematite, and leucoxene (after magnetite). Stage 3, chlorite$_2$ formed in spatial associated with gold (Fig. 2.13e) and in the chlorite$_2$-epidote shell surrounding the ore zone. Chlorite$_2$ mostly forms non-orientated clots and is commonly intergrown with epidote, and both minerals have irregular (partly resorbed) grain shapes (Fig. 2.13f). Chlorite$_2$ is relatively Fe-rich (mainly at 25-30% $FeO_{total}$) brunsvigite to diabantite with intermediate $Al_2O_3$ (14-19 wt.%) and minor MnO (< 0.25 wt.%), and $TiO_2$ (< 0.2 wt.%) contents.

***Stage 4*** alteration is characterized by the formation of micro-veins of calcite-quartz±chlorite$_3$ that cut across the $S_1$ fabric (Fig. 2.12e), as well as the continued formation of clay minerals. It is important to note that such veinlets are relatively uncommon, and carbonate growth during stage 4 is not pervasive. Mg-rich stage 4 chlorite$_3$ is locally intergrown with calcite, and is Fe-poor (~10-35% $FeO_{total}$) diabantite to penninite characterized by a low $Al_2O_3$ (13-14 wt.%) contents without MnO or $TiO_2$. Stage 4 veins are associated with the deposition of minor gold, bismuth selenide, chalcopyrite (Fig.13h), pyrite and rare Cu-Pb-Bi selenides that resemble junoite ($Pb_3Cu_2Bi_8(S,Se)_{16}$), cerromojonite ($CuPbBiSe_3$) and clausthalite (PbSe). Stage 4 calcite is generally pure $CaCO_3$, but occasionally contains up to 0.5 wt.% MnO.

***Stage 5*** alteration postdates mineralization and involved the localised growth of late-$D_3$, pale pink feldspar and minor quartz, magnetite, specularite, and titanite (Fig. 2.12f). Feldspar alteration is concentrated along fracture zones that vary in width from a few decimeters to over 20 m, and it resulted in the formation of vein- or dyke-like features (Fig. 2.12f). These are common in both hanging wall and footwall sequences. Assay values from drill core indicate that stage 5 feldspar veins and dykes do not contain gold, and where stage 5 veins intersect mineralization, gold was depleted.

The youngest hydrothermal event at Tick Hill, defined as ***Stage 6***, involved the formation of carbonate-quartz-clay assemblages along late veins and $D_4$ faults (Fig. 2.7h). In drill core, stage 6 alteration occurs in both footwall and hanging wall sequences. The veins commonly constitute infill along fault breccia with vuggy quartz, calcite, green clay minerals and minor pyrite.

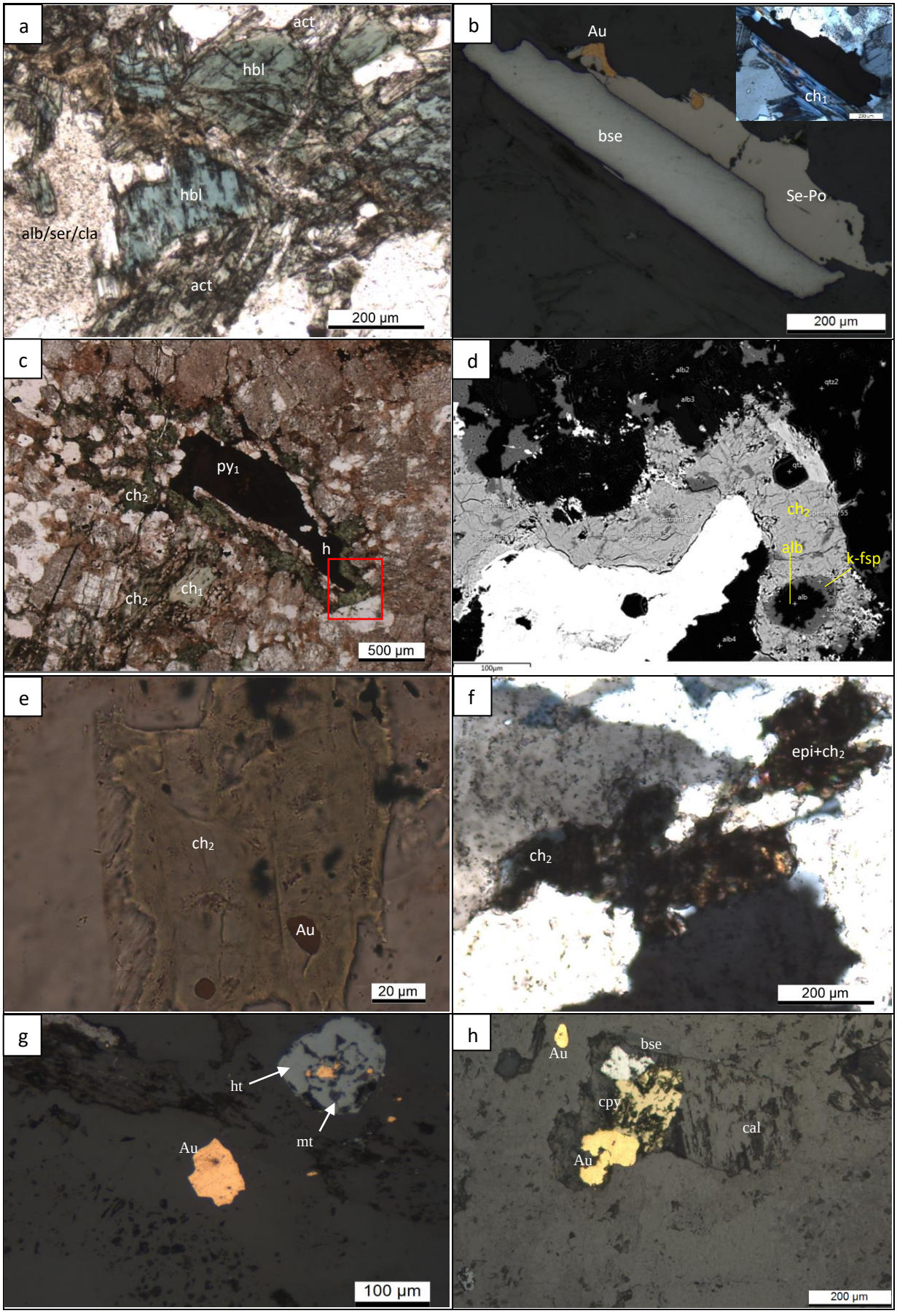
a
act
hbl
hbl
alb/ser/cla
act
200 µm
b
Au
ch1
bse
Se-Po
200 µm
c
py1
ch2
h
ch2
ch1
500 µm
d
alb2
alb3
qtz2
ch2
alb
k-fsp
alb4
100µm
e
ch2
Au
20 µm
f
epi+ch2
ch2
200 µm
g
ht
mt
Au
100 µm
h
Au
bse
cpy
cal
Au
200 µm

*Figure 2.13. Thin section and SEM images of alteration assemblages associated with gold (including stages 1 to 4). (a) Stage 2 actinolite rimmed and replaced stage 1 hornblende that formed along micro veins, with stage 3 clay minerals replacing stage 1 and 2 albite. (b) Stage 2 chlorite$_1$ replacing earlier biotite and was associated with, gold, bismuth selenide (bse) and Se-pyrrhotite (Se-Po). (c) Zoned coronal reaction rim of stage 3 green chlorite (ch$_2$), albite and quartz around an early coarse-grained pyrite (py$_1$). The matrix assemblage preserves earlier, stage 2 chlorite$_1$ (ch$_1$); the red box shows the area shown in (d). (d) SEM image showing more details of the reaction textures in (c) with early stage 3 albite inter-grown with chlorite$_2$ being replaced by later stage 3 K-feldspar. (e) Inclusion of fine-grained gold inside stage 3, chlorite$_2$ (ch$_2$). (f) Stage 3, chlorite$_2$ (ch$_2$) intergrown with epidote (epi). (g) Reflected light image of gold (Au) associated with stage 2 and 3 hematite (ht) after stage 1 magnetite (mt). (h) Stage 4 gold (Au), chalcopyrite (cpy) and bismuth selenide (bse) intergrown with calcite (cal; reflected light).*

## 5. Discussion

Since its discovery, intensive exploration in the region around Tick Hill has demonstrated that the deposit has no obvious extensions and, therefore, appears to be unique. What makes it different from other gold deposits in the Mt Isa Block is the high-grade, concentrated nature of the gold mineralization hosted in high-grade metamorphic rocks, the virtual lack of significant enrichment in other metals, the low sulfide content, and the presence of Bi-selenides. As such Tick Hill does not comfortably match the ore deposit models for either gold-rich IOCG deposits (e.g. Williams et al., 2001, 2005; Groves et al., 2010; Duncan et al., 2014) or orogenic lode gold occurrences (e.g. Goldfarb et. al., 2005; Danero et al., 2013).

In mapping the deposit and its associated structure, paragenesis and alteration assemblages a number of controlling factors have been identified that influence how gold-bearing fluids at Tick Hill may have moved to trapping sites, and how these fluids interacted with the host rock to deposit gold. These controls include lithological and structural controls as well as the nature of the far field stress, and the potential role of intrusive activity.

One important and puzzling feature about the Tick Hill deposit is the evidence for texturally early ($D_{1-2}$) and late ($D_3$) gold, together with indications that early gold and sulfide mineralization may have been remobilized (Fig. 2.9), which has led to a variety of mineralization concepts in past exploration campaigns (Tedman-Jones, 2001). The implications for the timing and origin of the Tick Hill deposit will be discussed in more detail below.

When discussing the mineralization events we will make reference to early and late gold. With respect the late gold phase it is important to bear in mind that the evidence shows that gold was mobile during $D_3$ stages 2-4, and that early gold was remobilized. However, we cannot be certain that the late gold stage involved the introduction of new gold.

### *5.1. Controls on the distribution of mineralization at Tick Hill*

#### *5.1.1. Lithological controls*

Mineralization at Tick Hill is not restricted to any one stratigraphic horizon, and the high-grade ore envelope transgresses different lithologies including quartzite, quartz-feldspar mylonite, calc-silicate gneiss, amphibolite and biotite schist (Fig. 2.3). All of these lithologies are characterized by strong-silicification that predated the main stage of mineralization. Thus, from a litho-chemical perspective there does not appear to be a single lithology (e.g., an Fe-rich lithology) that was especially conducive to the precipitation of gold, i.e. it is unlikely that chemical interaction between the host rock and a ligand carrying the gold was of great importance in trapping gold. Having said this, the lithologies in the area contain magnetite, in places at high concentrations, and the high-grade ore zone is characterized by a clear overprint of hematite replacing magnetite. Much of this magnetite formed early (during $D_1$ and $D_3$ stage 1 alteration; Table 2.1) as the product of metamorphism and early metasomatism, and its presence clearly played a role in the hematite alteration, and by extension, possibly gold. Thus, early gold precipitation during $D_1$ may have involved a reaction between magnetite and the altering high temperature fluids, but direct textural evidence for this has not been found.

The most characteristic feature of the high-grade ore zones in all lithologies is the high degree of silicification, which occurred both early ($D_1$) with silicification concentrated along the hanging wall quartzite and late ($D_3$) with the formation of a dense network of syn-$D_3$, laminar veins that are mostly thin (< 0.5 cm) and both parallel and transecting the dominant underlying $S_1$ mylonitic fabric. The fine, laminar $D_3$ veins have the appearance of quartz ribbon grains thereby masking the extent of their development in quartz-feldspar mylonite. Sodic, and potassic alteration with the development of albite and later K-feldspar-sericite was part of this process. In most places micro-fractures associated with the veining were healed, but their imprint remains visible as trails of fluid inclusions, alteration minerals, and gold grains.

Thus, the main lithological control on the configuration of the deposit with respect to the late gold stage and the lower temperature $D_3$ alteration events appears to have been mechanical in nature, in which strongly silicified, and, therefore, more competent lithologies were preferentially fractured. The competency of the lithologies resulted in part from the high-grade metamorphic nature (i.e. coarse-grained, granoblastic, mica-poor) of the rock in combination with the effects of at least two periods of pervasive silicification (early $D_1$ and early $D_3$) that affected the ore zone prior to $D_3$ fracturing and mobilization of the gold.

#### *5.1.2. Structural controls*

The geometry of the Tick Hill deposit is controlled by structures. $D_{1,2}$ shearing, folding and transposition led to the formation of tight intrafolial folds and the foliation truncation plane, which occur as macroscale shear bands; a phenomenon common in high-grade gneiss belts (e.g. Dirks and Wilson, 1995; Passchier and

Trouw, 2005). It also included the formation of laterally discontinuous mylonitic quartz-rich zones interpreted as silicified and altered, syn-$D_1$ shear horizons (e.g. Laing, 1993; Tedman-Jones, 2001) represented in Tick Hill by the hanging wall quartzite. These structures provided the architecture on which the gold mineralization was imprinted.

On the scale of the deposit (i.e. 100 m scale) the distribution of the ore zone coincided with a $D_1$ foliation truncation plane (Fig. 2.3), and early gold was probably concentrated along this surface. The $D_1$ foliation truncation plane was reactivated during $D_3$, as part of a network of faults and veins that created the fluid pathways through which later hydrothermal fluids were channeled that had the capacity to remobilize or transport gold.

Exploration reports for the deposit have suggested that the linear, east-northeast-plunging, high-grade ore zone parallels the dominant mineral elongation lineation ($L_{1x}$) and this has been used as an argument for early gold mineralization (e.g. Choy, 1994; Oliver, 1998). Our observations indicate that the linear high-grade ore envelope more-or less parallels the $L_{1x}$ mineral lineation, but it also coincides with the orientation of the intersection lineation between two sets of $D_3$ faults and associated veins (i.e. north-northeast-trending and east-trending sets; Fig. 2.6c). The main north-northeast-trending fault parallels the $D_1$ foliation truncation plane and the mylonitic fabric west of the fault, and the high-grade ore envelope coincides with it. The east-trending fracture set provides a second order (10 m scale) control on $D_3$ fluid migration. The coincidence of low-grade (<0.1 g/t) ore envelopes with some of these east-trending fractures away from the main ore zone, indicate that at least some of the gold moved along these fractures during $D_3$; the question is "by how much ?".

On the scale of individual outcrops, high-grade gold domains are dominated by numerous, laminar $D_3$ fractures that either parallel the main $S_1$ mylonitic fabric or occur as steep, east-trending partings to create the stock work vein pattern that is texturally associated with late gold. Gold occurs inside $D_3$ fractures and veins, and is commonly intergrown with $D_3$ alteration assemblages, linking the distribution of gold to $D_3$ structures as seen today on mm- to m-scales. However, coarse gold aligned in $S_1$ is commonly surrounded by a halo of fine gold, suggesting that early gold re-mobilized during $D_3$ did not necessarily travel far to be deposited again as late gold.

The textural observation that late gold may not have moved far, taken together with the spatial coincidence of the ore body with $L_{1x}$ and the $D_1$ foliation truncation plane, and the sharp boundary of the high-grade ore shell, indicate that gold remobilization during $D_3$ may only have had a limited spatial effect. It suggests that the large-scale distribution of gold at Tick Hill must be understood in terms of controlling $D_1$ structures.

### *5.2. The stress field during mineralization*

The nature of the stress field at the time of mineralization may have provided a further control on gold deposition. Early models for the Tick Hill deposit have suggested that the mineralization formed during $D_1$ in an extensional environment (e.g. Laing, 1993; Choy, 1994). Later, Tedman-Jones (2001) suggested that gold was controlled by activity on the Plumb Mt. and Mt. Bruce faults (Fig. 2.2a), due to the east-west compression during $D_3$ (Forrestal et al., 1998).

The strongly annealed and complex nature of $D_{1,2}$ structures and lack of kinematic indicators precludes reliable statements regarding the nature of the stress field during deposition of early gold. This is different for $D_3$ when late gold was deposited. The shear indicators that exist along the main north-northeast-trending $D_3$ fault suggest a sinistral-normal sense of movement, whilst the east-trending $D_3$ faults that are well exposed in the northwest corner of the pit, preserve clear normal components of movement (Fig. 2.7e). Given that the mineralization of late gold can be linked to these faults, both within the pit and in drill core, $D_3$ alteration and mineralization probably occurred during extension. The cause of extension at Tick Hill during $D_3$ is unresolved. It could reflect a localized effect, e.g. extension above an intrusive body, or it could have resulted from a regional extensional event.

### *5.3. The potential role of intrusions*

Exploration reports in the early 1990s have suggested that early gold mineralization was caused by the syn-$D_1$ emplacement of granites belonging to the Tick Hill intrusive suite (e.g. Tedman-Jones, 2021). This potentially included the quartz-feldspar mylonite that hosts much of the gold at Tick Hill. However, a genetic link between these strongly deformed and altered granites and early gold is hard to be proved other than pointing at a spatial correlation.

Arguments for possible intrusive activity during the formation of late gold are stronger. The occurrence of pegmatite veins and quartz-feldspar metasomatism in the high-grade ore zones, as well as the apparent association of gold with Bi-Cu and oxidizing fluids, can be interpreted as indications of intrusion-related gold mineralization (e.g. Thompson et al., 1999; Hart and Goldfarb, 2005). Aeromagnetic data collected by MIM during their exploration efforts in the 1990s showed that the Tick Hill orebody is located at the northeast margin of a 3x2 km, oval shaped magnetic low that was interpreted as a possible concealed intrusion (Nano, 1999), potentially linking mineralizing fluids to a granite intrusion at depth (Tedman-Jones, 2001). Other than the late pegmatite bodies describe here, no late-tectonic granite bodies were found in the area (Wyborn 1997; Laing, 1993). The late pegmatite intrusions around Tick Hill are granitic in composition and were emplaced during $D_3$. The stage 2 ($D_3$) feldspar-rich sheeted veins are similar in composition and relative timing as the late pegmatite veins, and they are common in drill core below the ore zone. These sheeted veins occur with fracture zones, and in part involved a metasomatic overprint of the surrounding gneiss. They share the same

deformation textures and are associated with similar alteration haloes as the late pegmatite bodies visible in the pit, and therefore, late pegmatite and late gold mineralization could be related to syn-$D_3$ igneous activity. Oxygen isotope data obtained from lithologies in and around the deposit, have been cited as evidence for an intrusive fluid (e.g. Choy, 1994). However, the $\delta\ ^{18}O_{VSMOW}$ values vary little (+10.2 to +12.9‰, Hannan, 1994) across a variety of rock types and veins, and they do not unequivocally reflect a magmatic source (e.g. Oliver et al., 2004).

A further argument that can be made for the possible involvement of an intrusive body at depth during late gold mineralization is the stockwork-like geometry of the fracture-networks and veins that host the gold at Tick Hill (Figs. 2.7c,e). Vein distribution patterns can reflect the broader geological setting during fluid migration. For example, intrusion-related, low- and high-sulfidation gold deposits that formed from fluids released by a causative intrusion typically display widespread stockwork veining across all lithologies (Corbett and Leach, 1998; Thompson et al., 1999; Corbett 2002; Rowe and Zhou, 2007; Goldfarb and Groves, 2015; Blenkinsop et al., 2020), rather than showing a systematic distribution of secondary structures near a master fault typical for orogenic gold deposits (e.g. Colvine et al., 1988; Goldfarb et al., 2005; Dirks et al., 2013). At Tick Hill, the mineralized $D_3$ veins, fracture networks and associated breccia zones are highly localized and stock-work like, whilst any through-going controlling $D_3$ shear zones are absent. Additionally, the five different stages of alteration and veining observed during $D_3$, suggest that brecciation and fracturing was a process that repeated itself several times, and involved a number of fluid pulses as the temperature of the altering fluid was cooling (Table 2.2). These observations are consistent with the presence of an igneous intrusion below Tick Hill, which could have driven episodic fluid flow through a network of $D_3$ structures and remobilized early gold, and/or introduced late gold.

### *5.4. Timing of mineralization*

Although most of the mineralization at Tick Hill when viewed on mm- to m- scales is related to $D_3$ fracture zones and associated laminar veins and quartz-albite-hematite-chlorite alteration (Table 2.2), not all observations fit this pattern. In particular, the presence of coarse-grained, granoblastic gold inclusions in seemingly unaltered peak-metamorphic hornblende and clinopyroxene grains that are aligned within $S_1$ contradicts $D_3$ gold mineralization. The presence of early gold in peak-metamorphic minerals was cited by Choy (1994), and has led to speculation during the early exploration stages that the mineralization must have predated the main $D_{1\text{-}2}$ events (Laing, 1993; Oliver, 1998; Tedman-Jones, 2001). In various exploration reports, it was suggested that the original source of mineralization could have been sedimentary-alluvial, syn-sedimentary epithermal, or associated with early stage intrusions that were subsequently sheared and mylonitised (Laing, 1993; England, 1993, 1995; Choy, 1994; Oliver, 1998). It is worth looking at each of these scenarios.

If a significant amount of the gold formed prior to or during $D_1$ it is hard to explain the highly concentrated nature of the mineralization considering the intensity of the $S_{1-2}$ mylonitic, transposition fabric and $D_3$ metasomatic overprint, unless the early gold forming event itself was highly localized. Regional exploration along strike, in litho-stratigraphic units that are similar to those hosting mineralization at Tick Hill, have not yielded any significant gold enrichment. This would make it unlikely that a significant amount of the gold at Tick Hill would have formed as alluvial gold in a sedimentary environment, or that it was associated with early intrusions, since both of these mechanisms would have likely resulted in a more dispersed distribution of early gold (e.g. Robb and Robb, 1998; Hart and Goldfarb, 2005; Tucker et al., 2016).

The most plausible explanation for the confined early deposition of gold, although based on limited evidence, has been the suggestion that gold was deposited from magmatic fluids in an extensional fault jog along $D_1$ shears that are represented by the quartzite ridges (e.g. Laing, 1993, Oliver, 1998; Tedman-Jones, 2001), with fluids moving along the $L_{1x}$ mineral elongation direction. This would have happened at the same time that granite was emplaced, which is represented by the quartz-feldspar mylonite that hosts much of the mineralization. Mapping of the quartzite ridges in the Tick Hill area has demonstrated that many of them transgress the dominant gneissic layering, and are strongly metasomatised (e.g. magnetite rich) with lensoidal geometries, gradational margins and fringed terminations suggesting alteration fronts (Coughlin, 1993; Laing, 1993). Few unequivocal sedimentary structures have been described from any of the quartzite ridges in the region, and many are characterized by extensive micro-veining, brecciation and silicification, largely masked by later recrystallization and metasomatism. This is the case for the hanging wall quartzite at Tick Hill, which was, therefore, interpreted as a strongly silicified metasomatised $D_1$ shear zone with early gold enrichment accompanying silicification in a $D_1$ dilational jog (e.g. Coughlin, 1993; Laing 1993; Oliver, 1998).

In spite of overwhelming structural evidence that the host rocks are mylonitic, the laminate textures in the Tick Hill ore zone have also been interpreted as primary varve-like deposits from silica gels in an epithermal environment (e.g. England, 1995). This interpretation followed suggestions of an epithermal exhalative origin for the gold-rich IOCG deposits at Starra (e.g. Davidson et al., 1989) ~60 km east of Tick Hill, but there is no evidence to support this.

Given the intensity of the later deformation and $D_3$ metasomatism, it is impossible to confidently pick the exact model that resulted in the deposition of early gold at Tick Hill. Structural arguments presented above suggest that the large-scale geometry of the ore zone is primarily controlled by $D_1$ structural elements, and that $D_3$, whilst pervasive at outcrop scales, only resulted in localized remobilization of early gold. These observations suggest that most if not all the gold at Tick Hill is early, even though the bulk of the mineralization when viewed in drill core, hand specimen or thin section is hosted by $D_3$ structures, and has, therefore been remobilized from early gold.

### *5.5. Constraints on the mineralizing fluids and mineralization style*

One of the characteristic alteration features associated with late gold mineralization at Tick Hill is the destruction of the magnetic signature in the lithologies that host the gold, as a result of the replacement of $D_{1-2}$ and stage 1 magnetite by hematite (Fig. 2.8). The abundance of hematite over magnetite in association with gold reflects the strongly oxidized nature of the $D_3$ hydrothermal fluids. In spite of this, the immediate hanging wall to the orebody is strongly enriched in magnetite, but most of this magnetite was texturally early, and probably associated with the formation of early gold, and it predated the pervasive late alteration and gold mineralization.

Similar to magnetite, sulfides appear to have been affected and largely resorbed in the high-grade ore zones, presumably by the same late stage ($D_3$), hydrothermal fluids. Gold observed in stage 2 to stage 4 assemblages, occurs everywhere as free gold, readily visible under the microscope, and generally associated with little or no sulfide. In some of the more mafic lithologies (e.g. amphibolite-bearing calc-silicate), gold occurs in spatial association with trace amounts of pyrite, chalcopyrite and pyrrhotite, but these sulfides are typically irregular, strongly embayed, and skeletal in shape, although in some places gold is intergrown with newly formed subhedral pyrite or pyrrhotite. Instead, gold is more commonly associated with Bi-selenides. These observations suggest that most sulfides represent the remains of older grains that may have formed with early gold and predated late gold mineralization when sulfide was largely resorbed and removed from the high-grade ore-zones by S-under-saturated fluids.

Pyrite, chalcopyrite and pyrrhotite patches are common in amphibolite and amphibolitic calc-silicate units in the hanging wall and footwall to the deposit. Although there is no obvious metal enrichment other than gold within the ore zone itself, a weak Co (> 30 ppm) anomaly has been observed, whilst the immediate footwall to the high-grade mineralized zone, typically showed enrichment in Cu (> 200 ppm). On a local scale, Cu and Co show a poor spatial correlation with gold in assay data, whilst Co and Cu correlate with each other and with Ni. The observed Cu-Co enrichment correlates with chalcopyrite-pyrite mineralization in the footwall. What is not clear is whether this chalcopyrite-pyrite mineralization formed with the late gold as part of the mineralizing fluids, or whether Cu and Co were present in the host rock prior to oxidizing fluids leaching the host rock of its metals during $D_3$. In other words, similar to magnetite being largely destroyed by the late stage oxidizing fluids, sulfides in the host rocks may have also been destroyed with S and Cu and to a lesser degree Co being removed from the high-grade gold zone as early gold was remobilized at a more localized scale. The Cu-sulfides were subsequently redeposited along the edges of the mineralization, presumably as a result of the interaction of the mineralizing fluids with the ambient fluids. This would be consistent with the sulfide textures and the gold-only nature of the ore. It is also consistent with early gold being re-mobilised by the same fluids to be redeposited as late gold along $D_3$ structures.

Apart from hematite, the gold-rich zone is characterized by quartz-albite-oligoclase-K-feldspar-sericite alteration, which showed a temporal evolution from early sodic alteration dominated by albite (stage 1 and early stage 2) to later, more potassic alteration with the formation of K-feldspar and sericite (late stage 2 and stage 3). The ore zone is further characterized by a recrystallized granoblastic texture in quartzo-feldspathic rocks. The bulk of the gold as preserved today was deposited during $D_3$ in stage 2, with stage 3 and 4 mineralization being either due to the continued inflow of new gold, or the remobilization of stage 2 gold (Table 2.2). However, as argued above, even stage 2 gold probably largely originated from the remobilization of early gold, and little, if any, gold may have been introduced during $D_3$.

The alteration mineral assemblage that formed during stage 1 (i.e. magnesio-hornblende, albite, oligoclase) indicates that $D_3$ metasomatic events started at upper-greenschist facies conditions in the core of the alteration zone. The assemblages that formed during stage 2 (actinolite, albite, chlorite$_1$), stage 3 (chlorite$_2$, epidote, k-feldspar, sericite) and stage 4 (chlorite$_3$, calcite) indicate a progressive drop in temperature of the hydrothermal fluids. The intense hematite alteration, the formation of leucoxene and selenides, and the destruction of magnetite (Fig. 2.8) and sulfide indicate that the mineralized fluids were strongly oxidized and S-under-saturated during stages 2 and 3. Conditions may have varied somewhat with the localized formation of pyrrhotite after pyrite suggesting more reduced conditions in at least parts of the deposit. This type of textural variation could reflect the interplay of reduced mineralizing fluid with a more oxidized ambient fluid considering the regional prevalence of hematite as an alteration phase (e.g. Oliver, 1995; Skirrow and Walshe, 2002). The fact that carbonates are largely absent from the alteration assemblage would further suggest that the mineralizing fluids did not contain $CO_2$. These constraints on the fluid composition indicate that late gold was not transported as a bisulfide complex, but must instead have moved as halogen complexes at low pH conditions. This is likely to have involved chlorine as is common in IOCG deposits in the Mt Isa district and considering the presence of Cl in stage 1 amphibole (e.g. Williams et al., 2001, 2005; Williams and Pollard, 2001; Oliver et al., 2004). Thus, the late stage, low temperature mineralizing fluids that remobilized early gold during $D_3$ were saline and oxidized, a characteristic that has been linked to igneous activity (e.g. Oliver et al., 2004; Mark et al., 2006).

One conspicuous feature about the Tick Hill deposit is the presence of a range of selenide minerals and the corresponding general paucity of sulfides in direct association with gold. Selenide minerals are relatively rare in mineral deposits because Se, which is strongly chalcophile, readily substitutes for sulfur in sulfide minerals. Deposition of selenides, rather than substitution in e.g. pyrite or chalcopyrite, therefore, requires specific conditions, and the selenide mineral assemblage places constraints on the nature the ore forming fluids as well as physical conditions of formation (e.g. Simon and Essene, 1996; Simon et al., 1997; Cook et al., 2009; Cabral et al., 2017). Bi-Cu-Pb bearing selenide deposits with hematite and rare sulfides have been described from vein deposits in schists, where they typically formed at relatively low temperatures from highly oxidized saline fluids within the hematite stability field at a low sulfur fugacity (e.g. Simon et al., 1997; Cabral

et al., 2017). A high oxygen fugacity prevents the early incorporation of Se in sulfides and promotes the formation of selenides, which generally occurs between 65 and 300°C, and mostly below 150°C (Simon et al., 1997). Reconstructions of the palaeo-depth of most selenide-bearing deposits indicate that lithostatic pressures were probably less than 0.5 kbar (Simon et al., 1997). The formation of copper selenides require acidic or reducing environments (Cook et al., 2009). Thus, the presence at Tick Hill of Bi-Cu-Pb selenides in association with gold probably indicates a relatively shallow depositional depth at relatively low temperatures and further confirms the involvement of strongly oxidized, acidic, saline fluids in which gold and other metals (Bi, Cu, Ni, Co) were mobilized as chlorine complexes (Simon et al., 1997; Cook et al., 2009). Some of the selenides at Tick Hill contain minor Te as well, and the association Au-Bi-Te-Se, together with other chalcophile elements has been linked to a magmatic signature (e.g. Spooner 1993).

### *5.6. An alternative model for gold at Tick Hill; involvement of Kalkadoon basement*

The alteration assemblage and structural setting at Tick Hill display some similarities with IOCG deposits in the Eastern Fold Belt of the Mt Isa Block (e.g. Williams et al., 2005), but these mostly relate to $D_3$ alteration and the mobilization of late gold. Similarities include the strong structural controls on mineralization, the prevalence of sodic alteration predating late gold mineralization and the shift from sodic to more potassic alteration as gold deposition progresses, the presence of abundant hematite and magnetite together with chlorite in association with gold, and the involvement of oxidized, acidic saline fluids (Williams, 1998; Williams and Pollard, 2001; Oliver et al., 2004; Williams et al., 2005; Groves et al., 2010; Mclellan et al., 2010). But there are important differences with classic IOCG deposits in the eastern fold belt (e.g. Groves et al., 2010). These include the absence of any significant copper mineralization, or any other significant metal enrichment for that matter, the absence of significant sulfide mineralization, the presence of Bi-selenides, and the absence of large volumes of concomitant felsic or mafic intrusions in the area at least during $D_3$ (Oliver et al., 2004; 2008). The high-grade metamorphic nature of the host rock, high gold-grade mineralization and extremely restricted nature of the deposit also differ from IOCG deposits in the Eastern Fold Belt. Thus, the geological setting of Tick Hill does not provide an easy match with any existing deposit type in the Mt Isa Province.

When considering the Au-rich nature of the Tick Hill deposit, its association with Bi and Se and extensive hematite-chlorite alteration, the Tick Hill deposit displays many similarities with some of the high-grade gold deposits (e.g. Nobles Nob, Eldorado; Skirrow and Walshe, 2002; Groves et al., 2010) in the Tennant Creek area of the Northern Territory, Australia. It is instructive to investigate these similarities in more detail, as it has implications for how to interpret the origin and timing of mineralization at Tick Hill.

The Tennant Creek gold field includes a large range of Au-Cu-Bi deposits that vary significantly in Au:Cu ratios, Fe-oxide and sulfide mineralogy and isotope compositions, and include reduced Cu-rich, and oxidized Au-rich end-members (Skirrow and Walshe, 2002; Groves et al., 2010). The Cu-rich endmember

deposits have been considered as possible IOCG deposits (e.g. Skirrow, 2000; Williams et al., 2005). In contrast, the Au-rich end-member deposits do not comfortably fit in the IOCG family (Groves et al., 2010), but they compare favorably with Tick Hill (e.g. Groves et al., 2010). Mineralization in the Tennant Creek area comprises native gold, chalcopyrite, and a range of bismuth minerals including S-Se-Te-Cu-Pb-bearing Bi sulfosalts (Large, 1975; Wedekind et al., 1989; Skirrow and Walshe, 2002). The Au-rich deposits (e.g. Juno, Argo, Nobles Nob, Eldorado) tend to have minor to abundant hematite alteration of pre-existing magnetite and widespread chlorite, muscovite, pyrite alteration (Skirrow and Walshe, 2002). The mineralization is typically hosted by structurally controlled, magnetite/hematite-rich, hydrothermal replacement bodies referred to as 'ironstones' that formed at temperatures of 350-400°C and 2.5-5.0 kbar (Skirrow and Walshe, 2002). These 'ironstones' are hosted by ca. 1860 Ma, low-grade metasedimentary turbidites. The Au-Cu-Bi mineralization was introduced into the ironstone bodies at slightly lower temperatures (~300°C) during the regional Tennant Event at 1860-1845 Ma (Compston and McDougall, 1994; Skirrow and Walshe, 2002). The Au-rich deposits have been linked to the reactions between magnetite ironstone and oxidizing brines that mixed with pulses of intermediate-oxygen fugacity, low- to moderate-salinity ore fluids to deposit gold and Bi sulfosalts whereas Cu deposition was suppressed by increasing solubility of Cu in the mixed fluid (Skirrow and Walshe, 2002). Additional significant 'non-ironstone' deposits of Au-Cu-Bi mineralization occur within shear zones outside the ironstones (e.g. Orlando East, Navigator 6; Skirrow, 2000; Skirrow et al., 2019). Some of the shear zone hosted deposits were dated at ca. 1660 Ma and are thought to have formed through remobilization of the main ironstone-hosted Au-Cu-Bi ore bodies with Au moving up to hundreds of meters (Skirrow et al., 2019). A ubiquitous feature of the gold-bearing veins is the presence of chlorite alteration adjacent to the veins together with hematite, monazite and chalcopyrite.

At Tick Hill it would appear that highly oxidized, Bi-Se-bearing hydrothermal fluids were capable of transporting gold to its current depositional site. The presence of gold in hornblende and clinopyroxene grains that are aligned in the $D_1$ fabric, indicates that that this gold mineralization may originally have occurred early. If one considers the parallels that exist with the Tennant Creek gold field, we suggest that there is a genuine possibility that early high-grade Au-Cu-Bi mineralization of the oxidized Au-rich end-member type (Skirrow and Walshe, 2002) may have formed either before or during $D_1$. During $D_{1,2}$ this early gold mineralization was aligned with or formed in parallelism with $D_1$ structures and it overprinted syn-$D_1$ intrusions now preserved as quartzo-feldspathic mylonite. If this early gold mineralization was subsequently reworked and overprinted by low temperature hydrothermal fluids with the capacity to remobilize metals including gold, then the Tick Hill deposit could represent a remobilized, older high-grade gold deposit. The fluids involved in this remobilization were highly saline, oxidized fluids that gave rise to the extensive regional albite-hematite alteration in the area (e.g. Oliver 1995). These fluids would not necessarily have to be gold-rich, but could have scavenged their metal load from the older deposits in a way described for the late Au-vein deposits in the Tennant Creek area (Skirrow et al., 2019).

## 6. Conclusion

Four deformational events have been recorded at Tick Hill and the surrounding rocks including: (1) regional $D_1$ shearing resulting in the formation of mylonitic textures at high-grade metamorphic conditions; (2) $D_2$ upright folding that formed the Tick Hill syncline, again at high-grade metamorphic conditions; (3) $D_3$ oblique-normal faulting with extensional veining and widespread quartz-feldspar alteration near Tick Hill and subsequent regional red rock alteration; and (4) $D_4$ strike-slip faulting with cataclasite textures. The ore zone at Tick Hill parallels a $D_1$ foliation truncation plane that was reactivated during $D_3$ sinistral-normal faulting. Mineralization also approximately parallels the $L_{1x}$ mineral elongation lineation, and the intersection lineation between sets of $D_3$ faults, with localized brecciation along the faults increasing with depth.

Key features of gold mineralization at Tick Hill include: (1) the high-grade, coarse-grained, gold-only nature of the deposit most of which was deposited in its current textural position during $D_3$ faulting and associated alteration (late gold); (2) the presence of an early, pre- or syn-$D_1$ stage of mineralization (early gold); (3) the restricted nature of the deposit, with an abrupt boundary between mineralized and non-mineralized zones; (4) a paucity of sulfides and other metals in the ore zone together with the presence Bi-selenides in association with late gold; (5) a prevalence of magnetite and hematite, with hematite concentrated in the ore zone; (6) early ($D_1$) high-temperature alteration assemblages characterized by magnetite and quartz, possibly associated with early gold; (7) late ($D_3$) low-temperature alteration assemblages characterized by proximal amphibole, albite, hematite, chlorite, epidote, sericite, illite, and minor calcite, and associated with late gold; (8) proximal mineralization coincided with $D_3$ brecciation and intense silicification, bounded by a strongly silicified zone and surrounded by a chlorite-epidote shell; (9) the presence of abundant laminar quartz veins, locally forming breccia associated with late gold; (10) the involvement of strongly oxidized, acidic, saline, hydrous fluid during late ($D_3$) low-temperature alteration; and (11) a possible genetic relationship between post-tectonic pegmatite and late-stage alteration fluids.

In terms of alteration assemblages and structural setting the Tick Hill deposit shares many similarities with the ca. 1850 Ma, Au-Cu-Bi mineralization in the Tennant Creek area. In contrast, its high-grade gold-only nature, lack of significant Cu enrichment, presence of Bi-selenides and general absence of associated intrusions make it a unique deposit in the Mt Isa Block. Evidence of early mineralization and $D_3$ related remobilization of gold and sulfides suggest that early gold enrichment was responsible for the bulk of the mineralization and it was remobilized by later hydrothermal fluids to be deposited as late gold in suitable structural traps during $D_3$.

# References


Babo, J., Spandler, C., Oliver, N.H., Brown, M., Rubenach, M.J., Creaser, R.A., 2017. The high-grade Mo-Re Merlin deposit, Cloncurry district, Australia: Paragenesis and geochronology of hydrothermal alteration and ore formation. Econ. Geol., 112(2), 397-422.

Betts, P., Giles, D., Mark, G., Lister, G., Goleby, B., Ailleres, L., 2006. Synthesis of the Proterozoic evolution of the Mt Isa Inlier. Aust. J. Earth Sci., 53(1), 187-211.

Blake D.H., Bultitude R.J., Donchak P.J.T., 1982. Dajarra, Queensland 1:100000 geological map commentary. BMR Geol. Geophys., 225, 83pp.

Blake, D.H., 1987. Geology of the Mount Isa inlier and environs, Queensland and Northern Territory. BMR Geol. Geophys. Aust. Bull., 225, 1-83.

Blake, D., Steward, A., 1992. Stratigraphic and tectonic framework, Mount Isa. AGSO Bull., 243, 1-11.

Blenkinsop, Oliver, Dirks P.H.G.M., Nugus, Sanislav I.V., Tripp, G., 2020. Structural Geology applied to the evaluation of Hydrothermal Gold Deposits. SEG Reviews in Econ. Geol., 21, 1-23.

Cabral A.R., Ließmann W., Jian W., Lehmann B. 2017. Selenides from St. Andreasberg, Germany: an oxidised fve-element style of mineralization and its relation to post-Variscan vein-type deposits of central Europe. Int. J. Earth Sci. (Geol Rundsch), 106, 2359–2369. DOI 10.1007/s00531-016-1431-z.

Carson, C., Hutton, L., Withnall, I., Perkins, W., Donchak, P., Parsons, A., Blake, P., Sweet, I., Neumann, N., Lambeck, A., 2011. Summary of results: Joint GSQ-GA geochronology project, Mount Isa region, 2009–2010. Queensland Geological Record 2011/03.

Choy, D.K.W., 1994. The geology, structure, petrology, alteration and mineralization of Tick Hill, North-West Queensland. Master Thesis, Monash University, 220pp.

Colvine, A., Fyon, J., Heather, K., Marmont, S., Smith, P., Troop, D., 1988. Archean lode gold deposits in Ontario. Ontario Geological Survey, Miscellaneous Paper, 139, 136pp.

Compston, D.M., McDougall, I., 1994. 40Ar/39Ar and K-Ar age constraints on the Early Proterozoic Tennant Creek Block, northern Australia, and the age of its gold deposits. Aust. J. Earth Sci., 41, 609-616.

Cook N.J.; Ciobanu, C.L.; Spry P.G. , Voudouris P., 2009. Understanding gold-(silver)-telluride-(selenide) mineral deposits. Episodes 32(4), 249-263.

Corbett, G.J., Leach, T.M., 1998. Southwest Pacific Rim gold-copper systems: structure, alteration, and mineralization. Society of Economic Geologists, Special publication, 6, 237pp.

Corbett, G., 2002. Epithermal gold for explorationists. AIG News, 67, 1-8.

Coughlin, T.J., 1993. Burke River; QLD; EPM 9083; Tick Hill Enclave 1:10000 Geological Mapping Programme. Internal MIMEX Report, Record No. 8548, Mt Isa exploration office.

Davidson, G., Large, R., Kary, G., Osborne, R., 1989. The BIF-hosted Starra and Trough Tank Au-Cu mineralization: A new stratiform association from the Proterozoic eastern succession of Mt. Isa, Australia. Econ. Geol., Monograph, 6, 135-150.

Day, R., Whitaker, W., Murray, C., Wilson, I., Grimes, K., 1983. Queensland Geology: A companion volume to the 1: 2,500,000 scale geological map (1975). Publications of the Geological Survey of Queensland, 383.

Denaro, T.J., Randall, R.E., Smith, R.J., 2013. Chapter 10: Mineral and Energy Resources, in; Jell, P.A. (Eds): Geology of Queensland, Geological Survey of Queensland, Brisbane, pp 687-762.

De Jong, G.D., Williams, P.J., 1995. Giant metasomatic system formed during exhumation of mid-crustal Proterozoic rocks in the vicinity of the Cloncurry Fault, northwest Queensland. Aust. J. Earth Sci., 42(3), 281-290.

Dirks, P., Wilson, C., 1995. Crustal evolution of the East Antarctic mobile belt in Prydz Bay: continental collision at 500 Ma? Precambrian Res., 75(3-4), 189-207.

Dirks P.H.G.M., Charlesworth, E.G., Munyai, M.R., Wormald, R. 2013. Stress analysis, post-orogenic extension and 3.01Ga gold mineralization in the Barberton Greenstone Belt, South Africa; Precambrian Res.**,** 226, 157-184. DOI: 10.1016/j.precam res.2012.12.007.

Dirks, P., Sanislav, I., van Ryt, M., Huizenga, J., Blenkinsop, T., Kolling, L., Kwelwa, S., Mwazembe, G., 2019. The world class gold deposits in the Geita Greenstone Belt, northwestern Tanzania. Econ. Geol.

Dirks, P.H.G.M, Sanislav, I.V., van Ryt, M., Blenkinsop, T.G et al., 2020. The world-class gold deposits in the Geita Greenstone Belt, NW Tanzania. In: Geology of the World's Major Gold Deposits and

Provinces, Sillitoe, R.H., Goldfarb, R.J., Robert, F., and Simmons, S.F., editors: Society of Economic Geologists, Special Publication, 23, 163-183.
Downs, R.C., 2000. Notes Concerning Thickness Distributions of Upper and Lower Quartzite horizons at Tick Hill and Their Control on Gold Mineralization. A Down-Plunge Drill Target. Internal report to MIM Exploration Pty Ltd , (B)CD.060, Record No. 20322, Mt Isa exploration office.
Duncan, R.J., Stein, H.J., Evans, K.A., Hitzman, M.W., Nelson, E.P., Kirwin, D.J., 2011. A new geochronological framework for mineralization and alteration in the selwyn-mount dore corridor, eastern fold belt, mount isa inlier, australia: Genetic implications for iron oxide copper-gold deposits. Econ. Geol., 106(2), 169-192.
Duncan, R.J., Hitzman, M.W., Nelson, E.P., Togtokhbayar, O., 2014. Structural and lithological controls on iron oxide copper-gold deposits of the Southern Selwyn-Mount Dore Corridor, Eastern Fold Belt, Queensland, Australia. Econ. Geol., 109(2), 419-456.
England, R.N., 1993. Petrographic report for 35 samples from Tick Hill. Report to MIM Exploration Pty Ltd. ISAMISREP.018, Record No. 30874, Mt Isa exploration office.
England, R.N., 1995. The Tick Hill sedimentary exhalative gold deposit. Report to MIM Exploration Pty Ltd. ISAMISREP.023, Record No. 30881, Mt Isa exploration office.
Etheridge, M., Rutland, R., Wyborn, L., 1987. Orogenesis and tectonic process in the Early to Middle Proterozoic of northern Australia. Proterozic Lithospheric Evolution, 17, 131-147.
Forrestal, P., Pearson, P., Coughlin, T., Schubert, C., 1998. Tick hill gold deposit. Geology of the mineral deposits of Australia and Papua New Guinea. Australian Institute of Mining and Metallurgy, Carlton South, VIC, Monograph 22, 699-706.
Foster, D.R., Austin, J.R., 2008. The 1800–1610Ma stratigraphic and magmatic history of the Eastern Succession, Mount Isa Inlier, and correlations with adjacent Paleoproterozoic terranes. Precambrian Res., 163(1), 7-30.
Goldfarb, R.J., Baker, T., Dube, B., Groves, D.I., Hart, C.J., Gosselin, P., 2005. Distribution, character, and genesis of gold deposits in metamorphic terranes. Econ. Geol., 100th anniversary vol., 40, 407-450.
Goldfarb, R.J., Groves, D.I., 2015. Orogenic gold: Common or evolving fluid and metal sources through time. Lithos., 233, 2-26.
Groves, D.I., Bierlein, F.P., Meinert, L.D., Hitzman, M.W., 2010. Iron oxide copper-gold (IOCG) deposits through Earth history: Implications for origin, lithospheric setting, and distinction from other epigenetic iron oxide deposits. Econ. Geol., 105(3), 641-654.
GSQ, 2015. Hyperspectral data for drill hole TH007RD (71815), Tick Hill Deposit. Geological Survey of Queensland. https://minesonlinemaps.business.qld.gov.au/SilverlightViewer/Viewer.html?Viewer=momapspublic (access 30 April 2018)
Hannan, K., 1994. Tick Hill District quartz oxygen isotope results. Report to MIM Exploration Pty Ltd, Memo.1996/024, Record No. 18742, Mt Isa exploration office.
Hart C.J.R., Goldfarb, R.J., 2005. Distinguishing intrusion-related from orogenic gold systems. New Zealand Minerals Conference Proceedings, 2005, 125-133
Holcombe, R., Pearson, P., Oliver, N., 1991. Geometry of a middle Proterozoic extensional decollement in northeastern Australia. Tectonophysics, 191(3-4), 255-274.
Huston, D.L., Stevens, B., Southgate, P.N., Muhling, P. and Wyborn, L., 2006. Australian Zn-Pb-Ag ore-forming systems: a review and analysis. Econ. Geol., 101(6), 1117-1157.
Jébrak, M., 1997. Hydrothermal breccias in vein-type ore deposits: a review of mechanisms, morphology and size distribution. Geol. Rev., 12(3), 111-134.
Johnson, D., 2002. Tick Hill Abrief Review. Report to MIM Exploration Pty Ltd, ISAMISREP.208a, Record No. 31073, Mt Isa exploration office.
Kositcin, N., Bultitude, R.J., Purdy, D.J., 2019. Queensland Geological Record 2019/02. Summary of results. Joint GSQ-GA Geochronology Project: Mary Kathleen Domain, Mount Isa Inlier, 2018-2019. Queensland Geological Record 2019/02.
Mark, G., Oliver, N.H., Williams, P.J., 2006. Mineralogical and chemical evolution of the Ernest Henry Fe oxide–Cu–Au ore system, Cloncurry district, northwest Queensland, Australia. Miner. Deposita, 40(8), 769.

McLellan, J.G., Mustard, R., Blenkinsop, T., Oliver, N.H., McKeagney, C., 2010. Critical ingredients of IOCG mineralization in the Eastern Fold Belt of the Mount Isa Inlier: insights from combining spatial analysis with mechanical numerical modelling. PGC Publishing, pp. 233-255.

Laing, W.P., 1992. The metasomatic development of the quartz-feldspar laminate gold hostrock at Tick Hill, Illustrated. Report to MIM Exploration Pty Ltd., ISAMISREP.010; Record No. 30862, Mt Isa exploration office.

Laing, W.P., 1993. Geology of the Tick Hill region, Mount Isa, with implications for exploration. Report to MIM Exploration Pty Ltd., ISAMISREP.017; Record No. 30870, Mt Isa exploration office.

Large, R.R., 1975. Zonation of hydrothermal minerals at the Juno mine, Tennant Creek goldfield, central Australia. Econ. Geol., 70 (8), 1387-1413.

Le, T.X., Dirks, P.H.G.M., Sanislav I.V., Huizenga, J.M., Cocker, H., Manestar, G.N., 2021. Geochronological constraints on the geological history and gold mineralization in the Tick Hill region, Mt Isa Inlier. Under review.

MacCready, T., Goleby, B., Goncharov, A., Drummond, B., Lister, G., 1998. A framework of overprinting orogens based on interpretation of the Mount Isa deep seismic transect. Econ. Geol., 93(8), 1422-1434.

Mark, G., Oliver, N.H., Williams, P.J., 2006. Mineralogical and chemical evolution of the Ernest Henry Fe oxide–Cu–Au ore system, Cloncurry district, northwest Queensland, Australia. Miner. Deposita, 40(8), 769-801.

MIM, 1993. Geological maps of underground mine levels at Tick Hill Mine. Mount Isa Mines, data repository, Mt Isa exploration office.

MIM, 2000. Assay data for exploration drill holes from Tick Hill. Mount Isa Mines, data repository, Mt Isa exploration office.

Nano, S., 1999. Tick Hill geophysics, geology. Report to MIM Exploration Pty Ltd, Unnamed record, Mt Isa exploration office.

Nano, S., Croxford, B., Moloney, M., 2000. Poster of Tick Hill Petrology. Report to MIM Exploration Pty Ltd, Unnamed record, Mt Isa exploration office.

Neumann, N., Gibson, G., Southgate, P., 2009. New SHRIMP age constraints on the timing and duration of magmatism and sedimentation in the Mary Kathleen Fold Belt, Mt Isa Inlier, Australia. Aust. J. Earth Sci., 56(7), 965-983.

O'dea, M., Lister, G., Maccready, T., Betts, P., Oliver, N., Pound, K., Huang, W., Valenta, R., 1997. Geodynamic evolution of the Proterozoic Mount Isa terrain. Geological Society, London, Special Publications, 121(1), 99-122.

Oliver, N.H., Rawling, T.J., Cartwright, I., Pearson, P.J., 1994. High-temperature fluid-rock interaction and scapolitization in an extension-related hydrothermal system, Mary Kathleen, Australia. Journal of Petrology, 35(6), 1455-1491.

Oliver, N., 1995. Hydrothermal history of the Mary Kathleen Fold Belt, Mt Isa Block, Queensland. Australian Journal of Earth Sciences, 42(3), 267-279.

Oliver, N., 1998. Tick Hill - Altered and deformed granites and Corella metasediments. Report to MIM Exploration Pty Ltd (Email form), Unnamed record, Mt Isa exploration office.

Oliver, N., Pearson, P., Holcombe, R., Ord, A., 1999. Mary Kathleen metamorphic-hydrothermal uranium-rare-earth element deposit: Ore genesis and numerical model of coupled deformation and fluid flow. Aust. J. Earth Sci., 46(3), 467-484.

Oliver, N.H.S., Cleverley, J.S., Mark, G., Pollard, P.J., Fu, B., Marshall, L.J., Rubenach, M.J., Williams, P.J., Baker, T., 2004. Modeling the Role of Sodic Alteration in the Genesis of Iron Oxide-Copper-Gold Deposits, Eastern Mount Isa Block, Australia. Econ. Geol., 99(6), 1145-1176.

Oliver, N.H.S., Butera, K.M., Rubenach, M.J., Marshall, L.J., Cleverley, J.S., Mark, G., Tullemans, F., Esser, D., 2008. The protracted hydrothermal evolution of the Mount Isa Eastern Succession: A review and tectonic implications. Precambrian Res., 163(1), 108-130.

Page, R., 1978. Response of U-Pb Zircon and Rb-Sr total-rock and mineral systems to low-grade regional metamorphism in proterozoic igneous rocks, mount Isa, Australia. Journal of the Geological Society of Australia, 25(3-4), 141-164.

Page, R., 1983. Chronology of magmatism, skarn formation, and uranium mineralization, Mary Kathleen, Queensland, Australia. Econ. Geol., 78(5), 838-853.

Passchier, C., 1986. Proterozoic deformation in the Duchess belt, Australia: A contribution to the BMR Mount Isa regional tectonic history program. Geol. en Mijnbouw, 65, 47-56.

Passchier, C., Williams, P., 1989. Proterozoic extensional deformation in the Mount Isa inlier, Queensland, Australia. Geological Magazine, 126(1), 43-53.

Passchier, C., 1992. Geology of the Myubee area, Mt Isa Inlier, Queensland. Detailed studies of Mount Isa Inlier, pp. 199-208.

Passchier, C.W., Trouw, R.A., 2005. Microtectonics. Springer Science & Business Media, 366pp.

Robb, L.J., Robb, V.M., 1998. Gold in the Witwatersrand Basin in The Mineral Resources of South Africa (M.G.C. Wilson and C.R. Anhaeusser, eds.): Handbook, Council for Geoscience, 6, 294-349.

Rowe, R. , Zhou, X., 2007. Models and exploration methods for major gold deposit types. Proceedings of exploration, 7, 691-711.

Rutherford, N.F., 1999. Tick Hill Joint Venture; Burke River Region, Mt Isa - Cloncurry district, NW Qld; EPM 9083, 11012, 11013; First Annual report; Period ended Jan. 1st 1999. ISAMISREP.253, Record No. 31113, Mt Isa exploration office or https://qdexguest.dnrm.qld.gov.au/portal/site/qdex/search?REPORT_ID=30650 (access 12 Nov 2017)

Rutherford, N.F., 2000. Tick Hill Joint Venture ; Burke River Region, Mt Isa - Cloncurry district, NW Qld; EPM 9083, 11012, 11013; Second Annual Joint Venture Report; period ended Jan. 1st 2000. ISAMISREP.254. Record No. 31114, Mt Isa exploration office or https://qdexguest.dnrm.qld.gov.au/portal/site/qdex/search?REPORT_ID=31587 (access 12 Nov 2017).

Simon, G., Essene, E.J., 1996. Phase relations among selenides, sulfides, tellurides, and oxides; I, Thermodynamic properties and calculated equilibria. Econ. Geol., 91(7), 1183-1208.

Simon, G., Kesler, S.E., Essene, E.J., 1997. Phase relations among selenides, sulfides, tellurides, and oxides.II. Applications to selenide-bearing ore deposits. Econ. Geol., 92, 468–484.

Skirrow, R.G., 2000. Gold-Copper-Bismuth Deposits of the Tennant Creek District, Australia: A Reappraisal of Diverse High Grade Systems, nn: Porter, T.M. (Eds.), Hydrothermal Iron Oxide Copper-Gold & Related Deposits: A Global Perspective. Austral. Min. Found. Adelaide, pp. 149-160.

Skirrow, R.G., Walshe, J.L., 2002. Reduced and oxidized Au-Cu-Bi iron oxide deposits of the Tennant Creek inlier, Australia: An integrated geologic and chemical model. Econ. Geol., 97 (6), 1167–1202.

Skirrow R.G., Cross A.J., Lecomte A., Mercadier J., 2019. A shear-hosted Au-Cu-Bi metallogenic event at ~1660 Ma in the Tennant Creek goldfield (northern Australia) defined by in-situ monazite U-Pb-Th dating. Precambrian Res. 332, 105402. Doi 10.1016/j.precamres.2019.105402.

Spooner ETC (1993) Magmatic sulphide-volatile interaction as a mechanism for producing chalcophile element enriched, Archean Au-quartz, epithermal Au-Ag and Au skarn hydrothermal ore fluids. Geol. Rev., 7, 359–379.

Tedman, C.J., 1993. Gold dispersion and geochemistry at the Tick Hill gold deposit and implications for exploration, Mt Isa Inlier, NW Queensland. Master of Science, James Cook University, 122pp.

Tedman-Jones, C., 2001. Tick Hill core relogging review. Internal report to MIM Exploration Pty Ltd. Misc.2001/010, Record No. 30764, Mt Isa exploration office.

Thompson, J., Sillitoe, R., Baker, T., Lang, J., Mortensen, J., 1999. Intrusion-related gold deposits associated with tungsten-tin provinces. Miner. Deposita, 34(4), 323-334.

Tucker, R.F., Viljoen R.P., Viljoen M.J. 2016. A Review of the Witwatersrand Basin - The World's Greatest Goldfield. Episodes 39, DOI: 10.18814/epiiugs/2016/v39i2/95771.

Walters, S., Bailey, A., 1998. Geology and mineralization of the Cannington Ag-Pb-Zn deposit; an example of Broken Hill-type mineralization in the eastern succession, Mount Isa Inlier, Australia. Econ. Geol, 93(8), 1307-1329.

Watkins, R., 1993. Deformation, felsic magmatism and alteration associated with the Tick Hill Gold Deposit, NW Queensland, B.Sc. Hons. Thesis, Monash University.

Wedekind, M.R., Large, R.R., Williams, B.T., 1989. Controls on high-grade gold mineralization at Tennant Creek, Northern Territory, Australia. Econ. Geol., Monograph 6, 168-179.

Williams, P., 1998. Metalliferous economic geology of the Mt Isa eastern succession, Queensland. Aust. J. Earth Sci., 45(3), 329-341.

Williams, P.J., Pollard, P.J., 2001. Australian Proterozoic iron oxide-Cu-Au deposits: An overview with new metallogenic and exploration data from the Cloncurry district, northwest Queensland. Exploration and Mining Geology, 10(3), 191-213.

Williams, P.J., Dong, G., Ryan, C.G., Pollard, P.J., Rotherham, J.F., Mernagh, T.P., Chapman, L.H., 2001. Geochemistry of hypersaline fluid inclusions from the Starra (Fe oxide)-Au-Cu deposit, Cloncurry District, Queensland. Econ. Geol., 96(4), 875-883.

Williams, P.J., Barton, M.D., Johnson, D.A., Fontboté, L., De Haller, A., Mark, G., Oliver, N.H., Marschik, R., 2005. Iron oxide copper-gold deposits: Geology, space-time distribution, and possible modes of origin. Econ. Geol., pp 371-405.

Withnall, I., Hutton, L., 2013. Chapter 2: North Australian Craton, in: Jell, P.A. (Eds): Geology of Queensland. Geology of QUeensland, Geological Survey of Queensland, Brisbane, pp 23-112.

Wyborn, L., A.I., 1997. Dajarra 1:100,000 digital geology, part of Mt Isa geological digital dataset. Updated by Geological Survey of Queensland 2011, 2015 and 2018. http://pid.geoscience.gov.au/dataset/ga/30923 (access 10 Aug 2020).

Wyborn, L., Page, R., McCulloch, M., 1988. Petrology, geochronology and isotope geochemistry of the post-1820 Ma granites of the Mount Isa Inlier: mechanisms for the generation of Proterozoic anorogenic granites. Precambrian Res., 40, 509-541.

Xu, G., 1996. Structural geology of the Dugald River Zn-Pb-Ag deposit, Mount Isa Inlier, Australia. Ore Geol. Rev., 11(6), 339-361.